HE & VHE emissions from black-hole magnetospheres

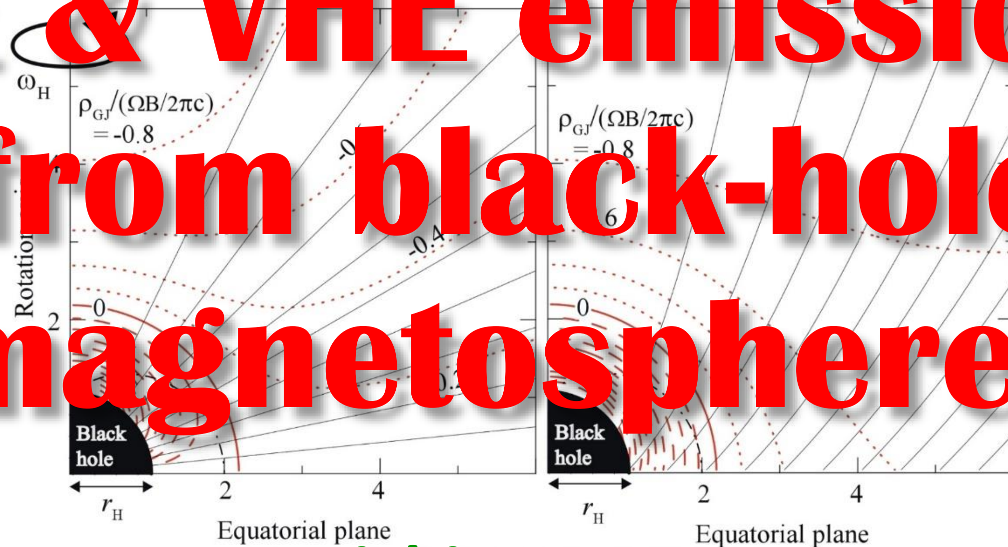

Side view of BH magnetosphere

Kouichi HIROTANI

ASIAA,Taiwan

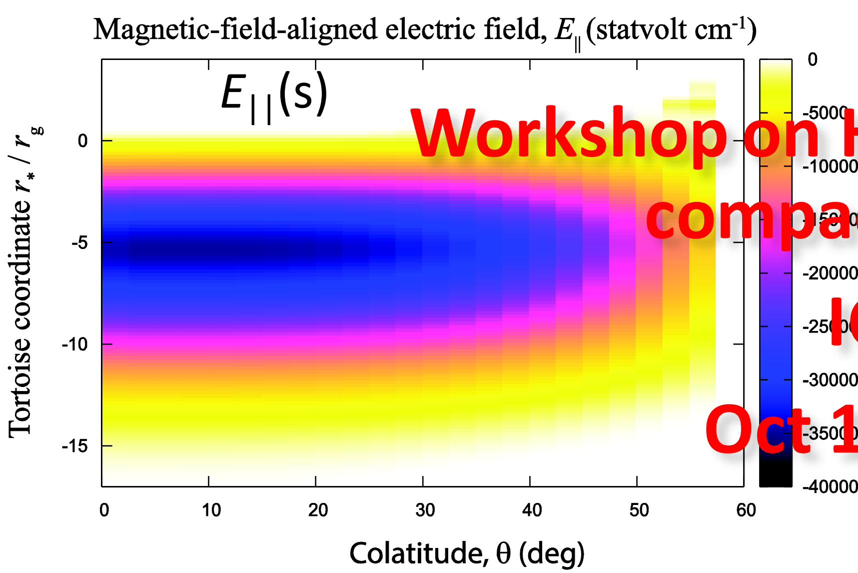

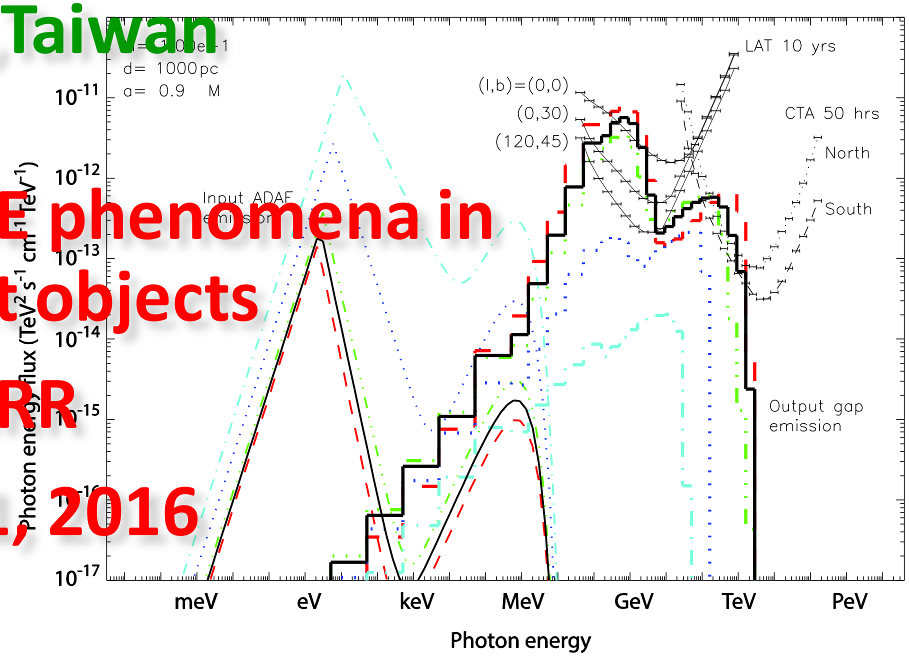

Workshop on HE phenomena in compact objects

ICRR

Oct 11, 2016

§ 1 Introduction

Accreting black holes (BHs) of arbitrary size can produce relativistic jets, which are observable from radio to VHE.

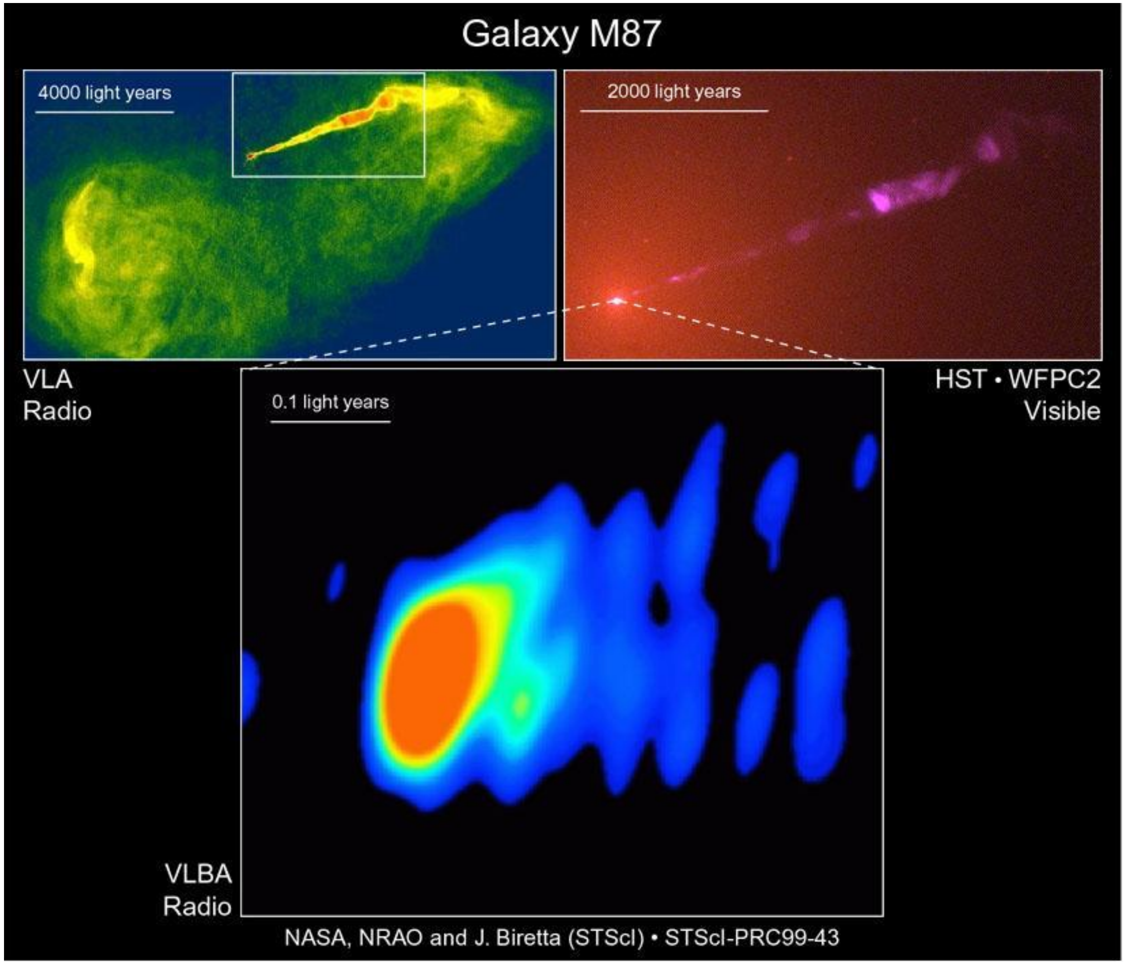

NASA, NRAO & Biretta (STSci), STSci-PROC99-43

§ 1 Introduction

Accreting black holes (BHs) of arbitrary size can produce relativistic jets, which are observable from radio to VHE.

Plausible mechanism of jet formation: Extraction of BH rotational energy thru Blandford-Znajek process.

(Blandford & Znajek (1976) MNRAS, 179, 433)

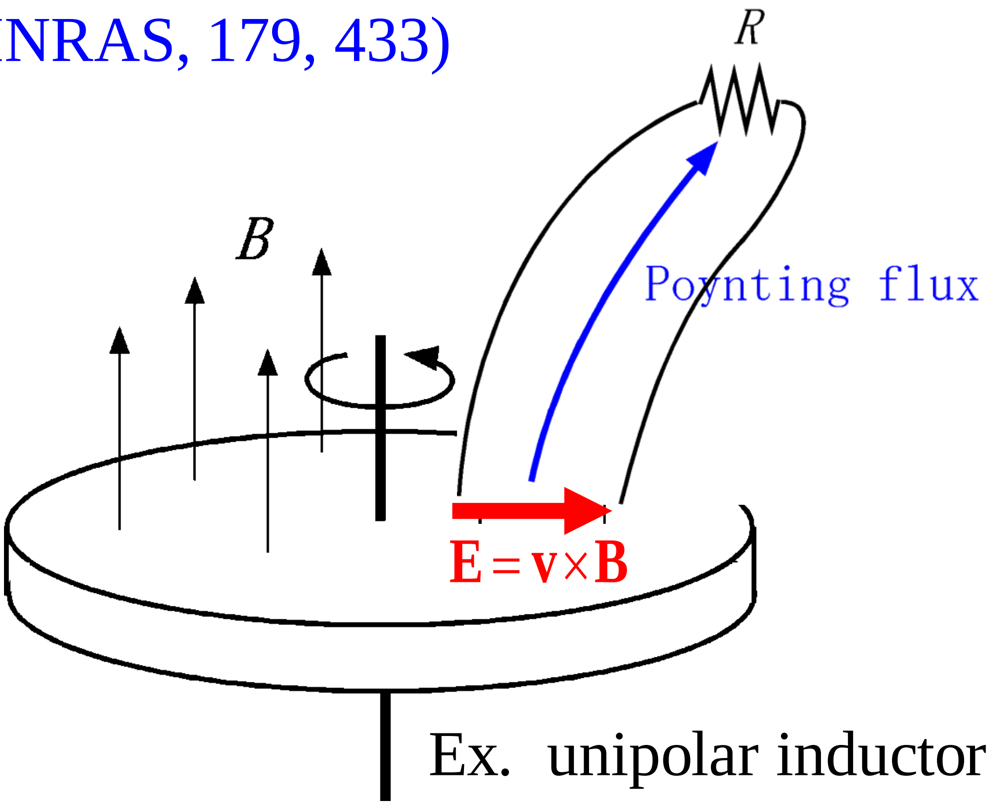

Ex. unipolar inductor

§ 1 Introduction

Accreting black holes (BHs) of arbitrary size can produce relativistic jets, which are observable from radio to VHE.

Plausible mechanism of jet formation: Extraction of BH rotational energy thru Blandford-Znajek process.
(Blandford & Znajek (1976) MNRAS, 179, 433)

In this EM process, **B** exerts counter torque on the event horizon to spin down the BH, launching Poynting-flux-dominated outflow (Koide + 2002, Sci 295, 1688).

§ 1 Introduction

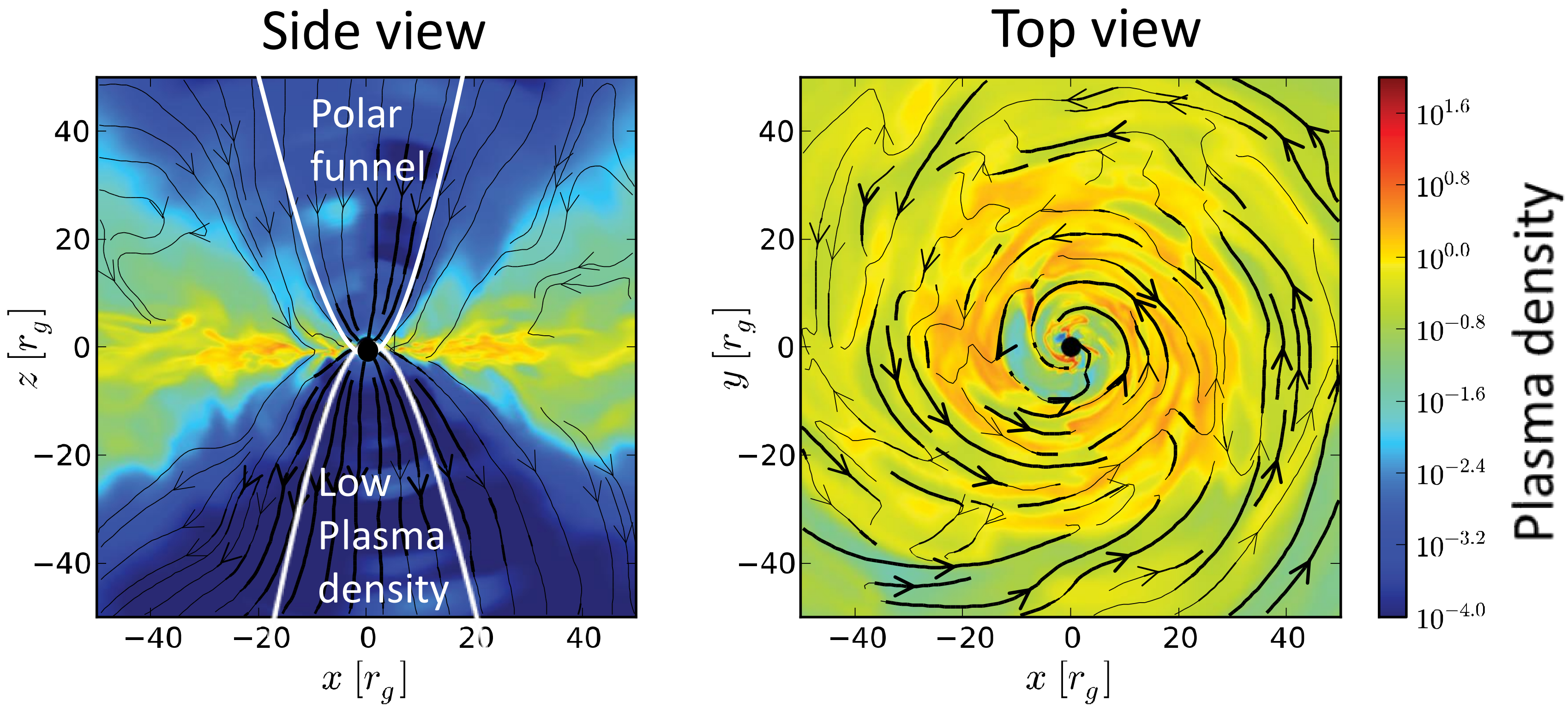

Avara + (2016, MNRAS 462, 636)

Indeed, genera-relativistic (GR) MHD simulations show steady, collimated, **B**-dominated jets in the polar region

(Mckinney & Gammie 2004, ApJ 611, 977; Hirose + 2004, ApJ 606 1083).

§ 1 Introduction

Even if the polar funnels are **B**-dominated, it is the electric current that sustains the EM power, and it is the charged particles that carry the current.

Causality requires that charges must flow into the horizon.

Accreting plasmas cannot penetrate into the funnels due to the centrifugal-force barrier.

Radiatively inefficient accretion flow (RIAF) cannot supply enough MeV photons that are capable of materializing as pairs in the funnels.

We need a process of plasma supply deep within the magnetosphere somewhere above the horizon.

§ 1 Introduction

To contrive a plasma source near the horizon, Beskin et al. (1992, Sov. Astron., 36, 642) proposed the BH gap model, extending the pulsar gap model (Cheng + 1986, ApJ 300, 500).

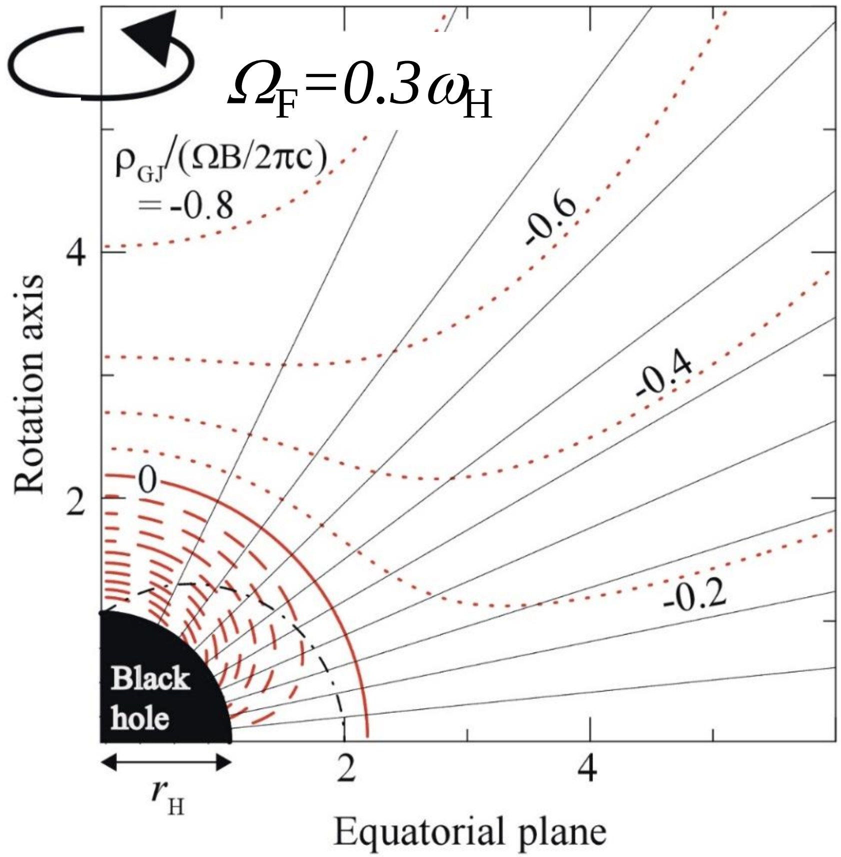

In BH magnetosphere, null surface is formed close to the $\Omega_F=\omega$ surface.

This surface (red solid curve) is located near the horizon due to the frame dragging effect.

§1 Introduction

To contrive a plasma source near the horizon, Beskin et al. (1992, Sov. Astron., 36, 642) proposed the BH gap model, extending the pulsar gap model (Cheng + 1986, ApJ 300, 500).

K.H. & Okamoto (1998, ApJ 497, 563) then showed that sufficient plasmas can be supplied via γ-γ pair production around super-massive BHs.

However, predicted γ-ray fluxes were undetectable, because they assumed high accretion rates (as in QSOs), which leads to a very thin gap width ($w \ll r_g$) along **B** lines, where $r_g = GMc^{-2}$.

§ 1 Introduction

Thus, Neronov & Aharonian (2007, ApJ 671, 85) and Levinson & Rieger (2011, ApJ 730, 123) revisited the BH gap model, adopting much thicker gap width ($w \sim r_g$) and examined M87* and Sgr A*.

Then Broderick & Tchekhovskoy (2015, ApJ 809, 97) showed that two-stream instability does not grow in BH gaps.

Subsequently, KH & Pu (2016, ApJ 818, 50) showed that a gap arises around the null-charge surface where the GR Goldreich-Julian (GJ) charge density vanishes, and that the null surface appears near the horizon due to frame dragging.

§ 1 Introduction

Today, we extend KH & Pu (2016) and apply the method to (mainly) stellar-mass BHs.

KH & Pu (2016)

Except for the GR GJ charge density, all other equations are solved in 1-D Newtonian limit.

This work

All equations are solved general relativistically on the 2-D poloidal plane. The predicted flux increases about 1.5 times compared to 1-D Newtonian approx.

§ 2 BH gap model

Around a rotating BH, gaps appear around the null surface that is located near the horizon. (Beskin + 1992)

Null surface is formed close to the $\Omega_F=\omega$ surface.

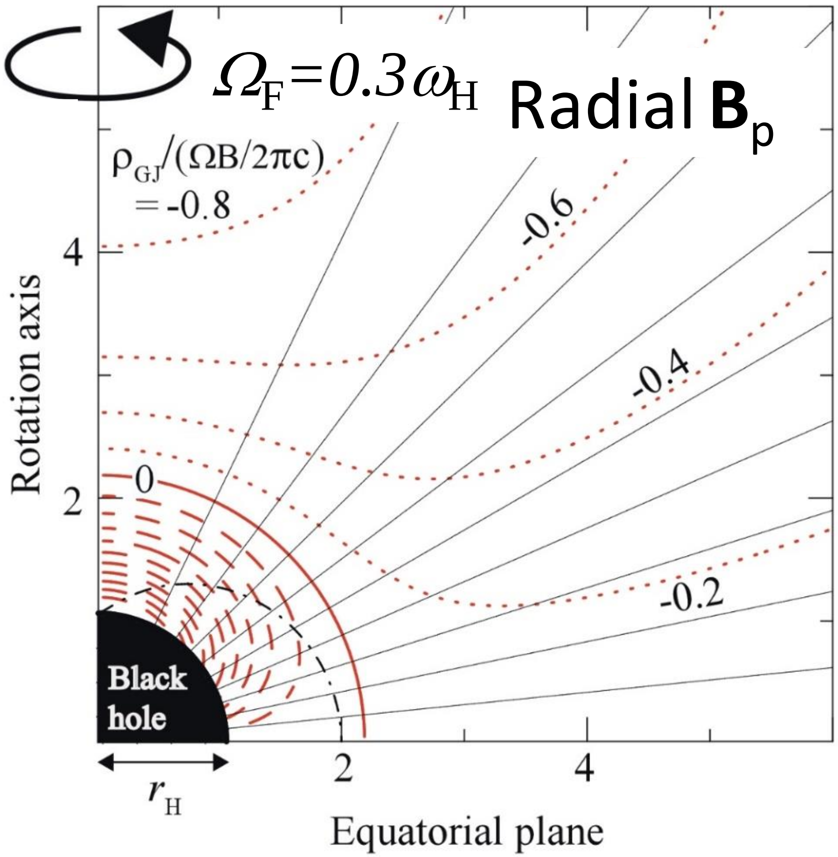

The GR Goldreich-Julian charge density:

$$\rho_{GJ} \equiv -\frac{1}{4\pi}\nabla\bullet\left(\frac{\Omega_F-\omega}{2\pi\alpha c}\nabla\Psi\right)$$

Ω_F: angular freq. of $\boldsymbol{B}$

ω: angular freq. of frame dragging

α: redshift factor (lapse function)

Ψ: magnetic flux function

$$\mathbf{B}_p=-\frac{e_\phi\times\nabla\Psi}{2\pi\varpi},\quad \mathbf{E}_p=-\frac{\Omega_F-\omega}{2\pi\alpha c}\nabla\Psi$$

§ 2 BH gap model

Its position little depends on $\mathbf{B}_p$ if $\partial\Omega_F / \partial\Psi \approx 0$.
We thus adopt a radial $\mathbf{B}_p$.

Null surface is formed close to the $\Omega_F = \omega$ surface.

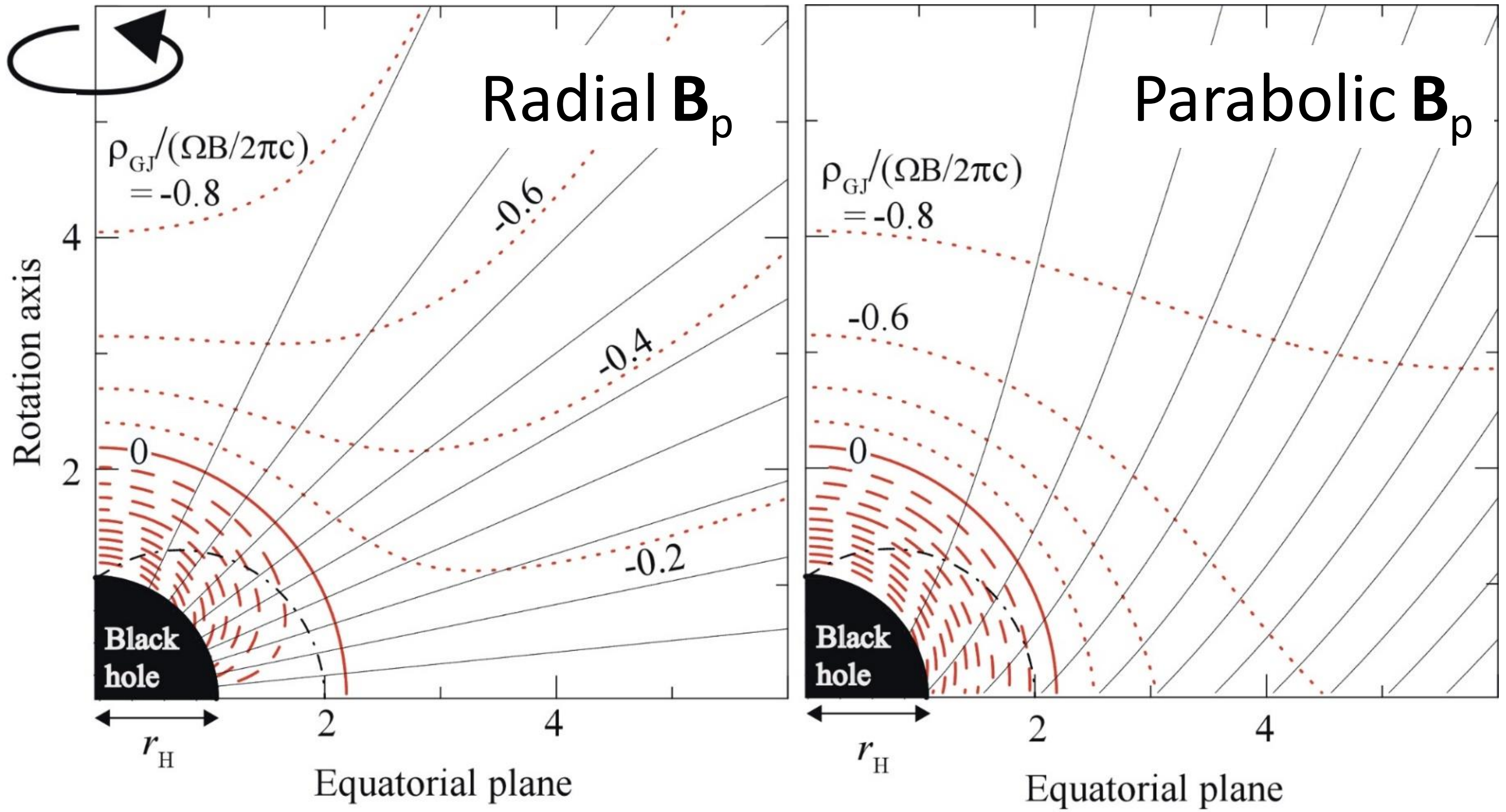

§ 2 BH gap model

Around a rotating BH, gaps appear around the null surface that is located near the horizon.

Within the gap, rotational energy of the BH can be partly dissipated as radiation.

Thus, the maximum gap luminosity is limited by the energy extraction rate from the rotating BH.

The EM extraction rate is given by

(Blandford & Znajek 1977, MNRAS 179, 433)

$$L_{\mathrm{BZ}} \approx 10^{45} \left(a / M \right)^2 M_9{}^2 B_4{}^2 \ \mathrm{ergs\ s}^{-1}$$

§ 2 BH gap model

Assuming $B \approx B_{\rm eq} = 4\times10^{8}\,\dot{m}^{1/2} M_1^{-1/2}$ G, we obtain

$$L_{\rm BZ} \approx 1.7\times10^{38} \left(a / \mathrm{M}\right)^2 \dot{m} M_1 \text{ ergs s}^{-1}.$$

$$\dot{m} = \dot{M} / \dot{M}_{\rm Edd}, \quad M_1 \equiv M / 10 M_\odot$$

The upper limit of $\dot{m}$ for a gap to appear is set by the condition that the magnetosphere becomes charge-starved, (Levinson & Rieger 2011, ApJ 730, 123)

$$\dot{m} > \dot{m}_{\rm up} = 3\times10^{-3} M_1^{-0.14}$$

If $\dot{m} > \dot{m}_{\rm up}$, ADAF MeV photons provide enough pairs via $\gamma\gamma \rightarrow ee$ (i.e., magnetosphere becomes force-free)

§ 2 BH gap model: general discussion

A gap ($E_{\parallel} \neq 0$) appears only for a low accretion rate,

$$\dot{m} < \dot{m}_{\mathrm{up}} = 3 \times 10^{-3} M_1^{-0.14}$$

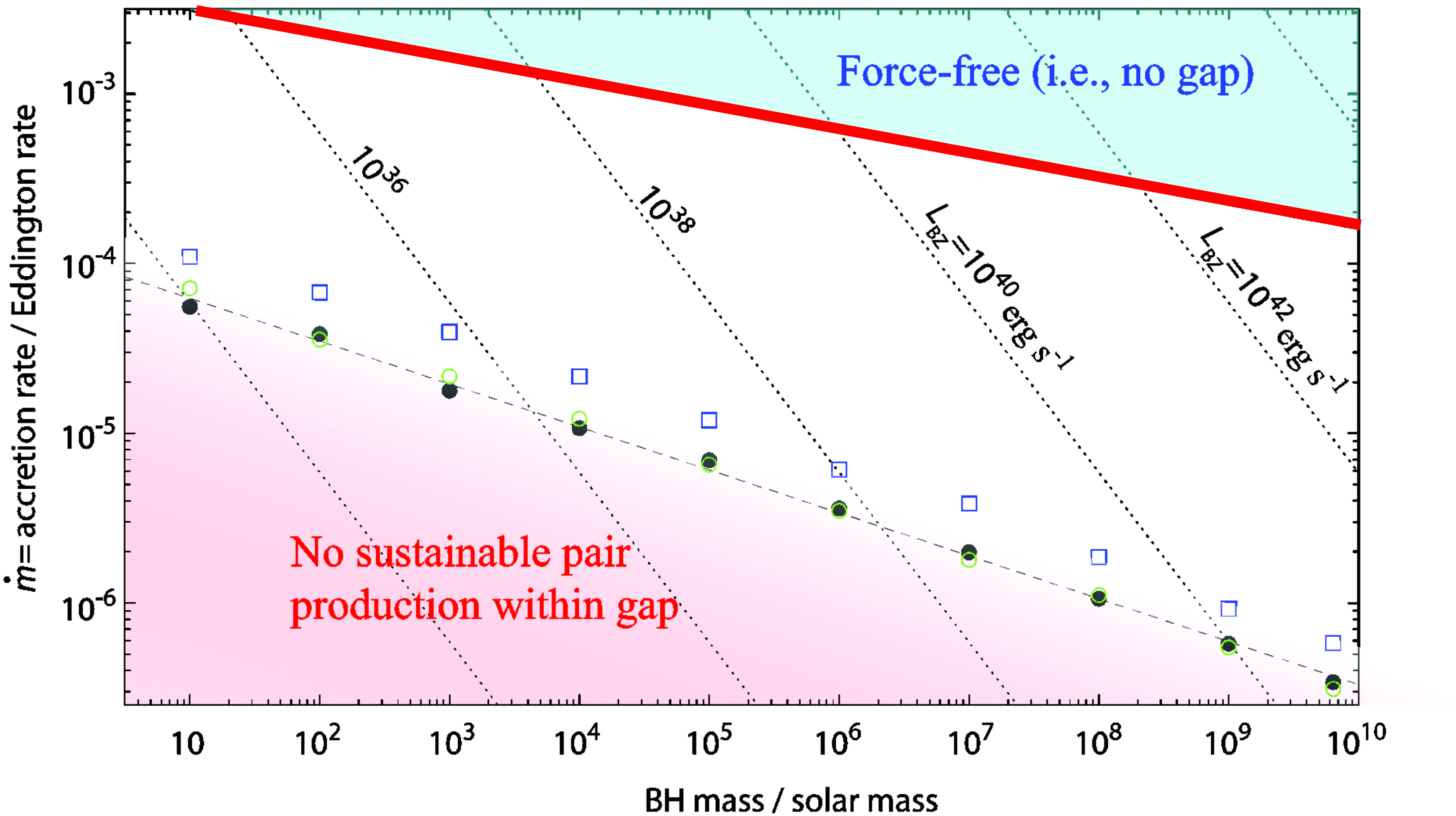

§ 2 BH gap model: general discussion

Substituting $\dot{m} \approx \dot{m}_{\rm up}$ into $L_{\rm BZ}$, we obtain the max. $L_{\rm gap}$,

(I) Stellar-mass BHs

KH + (2016b)

$$F_{\rm BZ} \approx 4.1 \times 10^{-9} M_1^{6/7} \left(\frac{d}{\rm kpc} \right)^{-2} \ \text{ergs s}^{-1}\text{cm}^{-2}$$

(II) Intermediate-mass BHs

$$F_{\rm BZ} \approx 2.1 \times 10^{-15} M_1^{6/7} \left(\frac{d}{10\rm Mpc} \right)^{-2} \ \text{ergs s}^{-1}\text{cm}^{-2}$$

(III) Super-massive BHs

$$F_{\rm BZ} \approx 3.0 \times 10^{-10} M_1^{6/7} \left(\frac{d}{10\rm Mpc} \right)^{-2} \ \text{ergs s}^{-1}\text{cm}^{-2}$$

§ 2 BH gap model: general discussion

Substituting $\dot{m} \approx \dot{m}_{\rm up}$ into $L_{\rm BZ}$, we obtain the max. $L_{\rm gap}$,

(I) Stellar-mass BHs

KH + (2016b)

$$F_{\rm BZ} \approx 4.1 \times 10^{-9} M_1^{6/7} \left(\frac{d}{\rm kpc} \right)^{-2} \ {\rm ergs\ s^{-1} cm^{-2}}$$

(II) Intermediate-mass BHs

$$F_{\rm BZ} \approx 2.1 \times 10^{-15} M_1^{6/7}$$

(III) Super-massive BHs

$$F_{\rm BZ} \approx 3.0 \times 10^{-10} M_1^{6/7} \left(\frac{d}{\rm 10Mpc} \right)^{-2} \ {\rm ergs\ s^{-1} cm^{-2}}$$

Stellar-mass or super-massive BHs are capable of emitting detectable BH gap emissions.

§ 2 BH gap model: general discussion

There is also a lower limit below which insufficient pair production prevents the formation of a stationary gap.

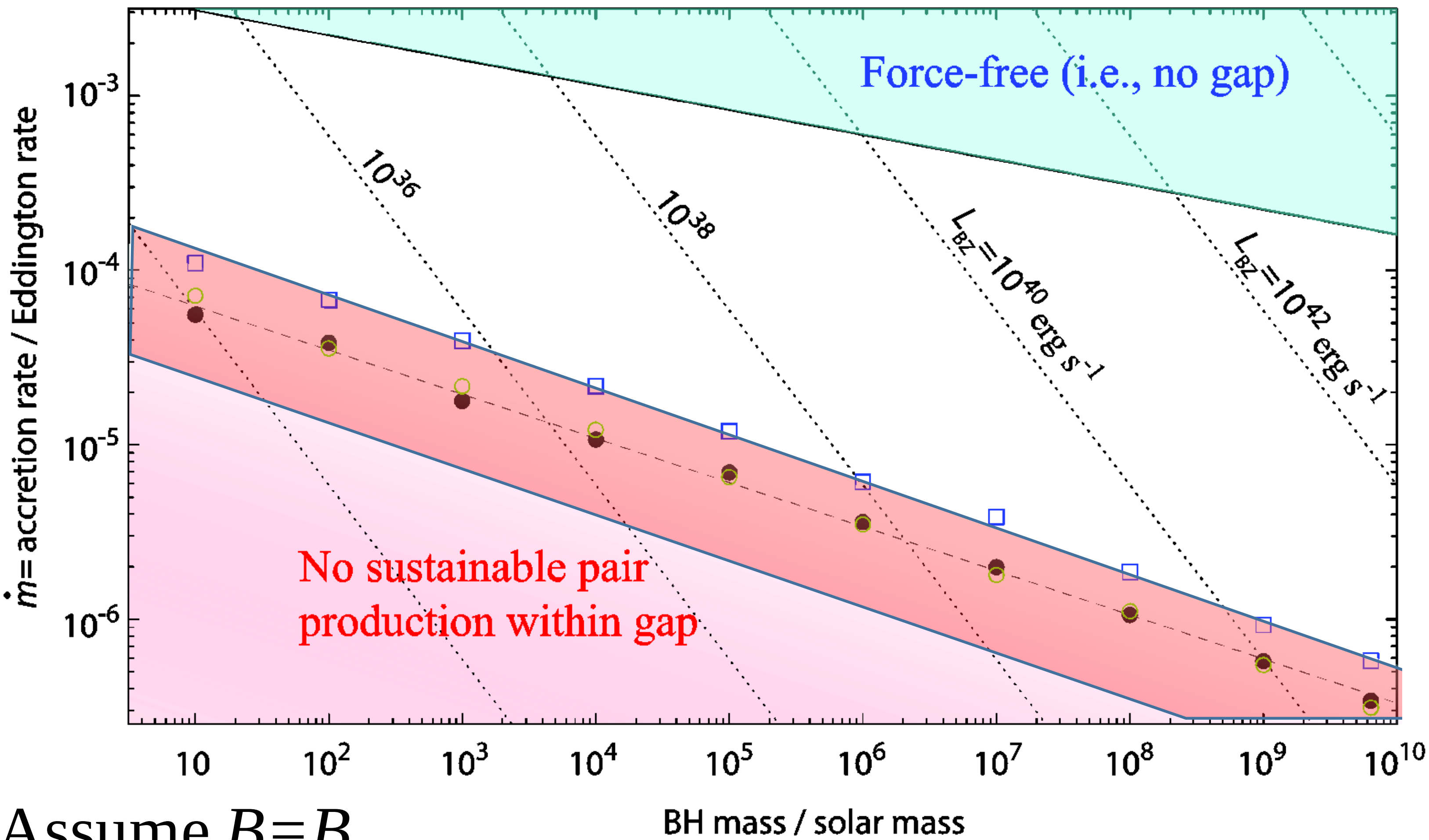

Assume $B=B_{eq}$

§ 2 BH gap model: general discussion

Gap exists between the upper & lower limits.
Let us begin with a stellar-mass case, $M=10M_{\odot}$.

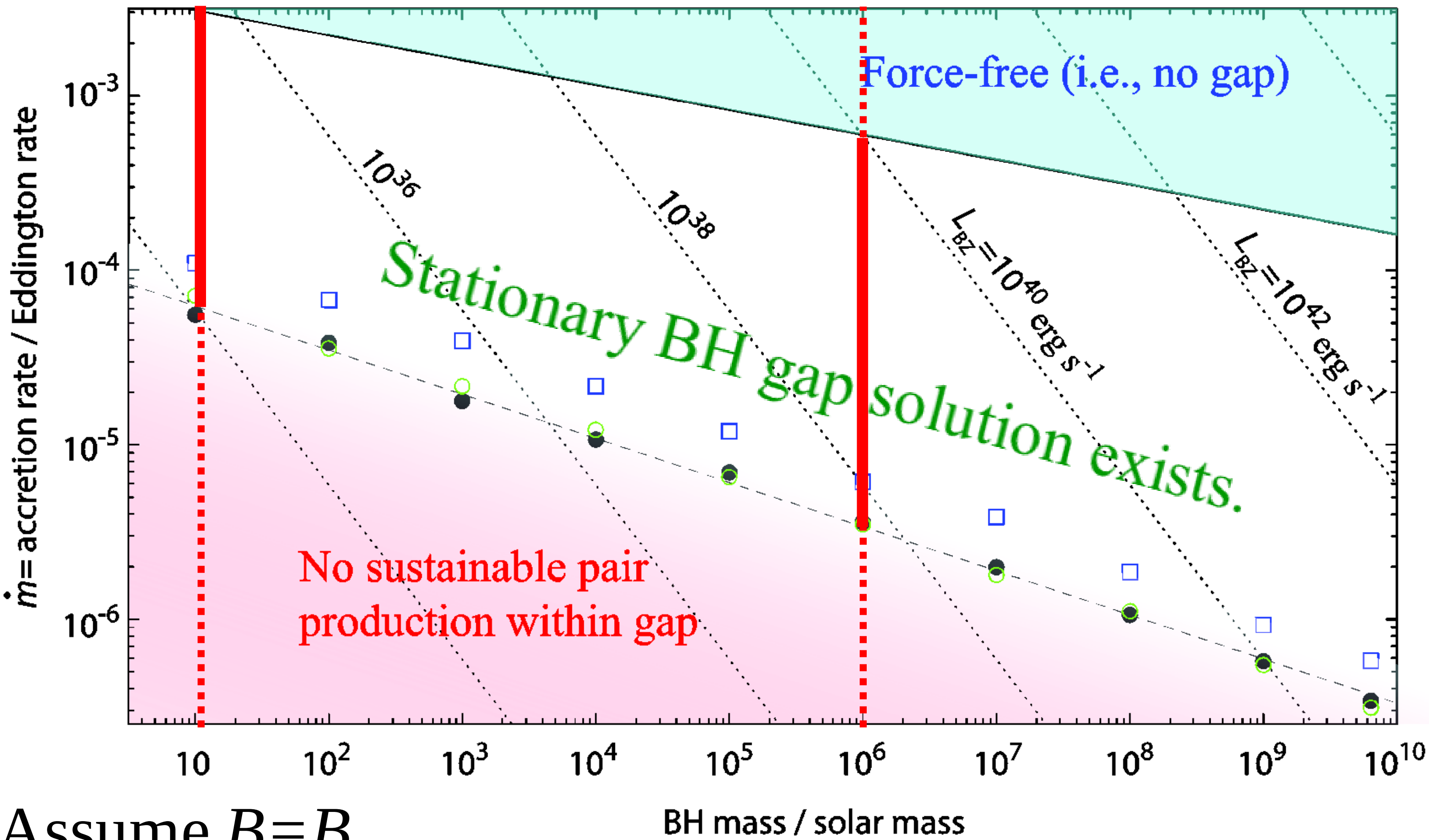

Assume $B=B_{eq}$

§ 3 Method

In the same way as in pulsar outer gap models, BH gap appears around the null surface and is quantified by solving pair-creation cascade consistently.

$e^{\pm}$'s are accelerated by $E_{\parallel}$

Relativistic e^+/e^- emit γ-rays via synchro-curvature, and IC processes

γ-rays collide with soft photons/B to materialize as pairs in the accelerator

§ 3 Method: Basic equations

Beskin + (1992)

Poisson eq. From $\nabla \bullet E = 4\pi\rho$, we obtain

$$\nabla \bullet E_{\parallel} = 4\pi(\rho - \rho_{\mathrm{GJ}}),$$

where

$$\rho_{\mathrm{GJ}} \equiv -\frac{1}{4\pi}\nabla \bullet \left(\frac{\Omega_{\mathrm{F}} - \omega}{2\pi\alpha c} \nabla\Psi \right), \quad \alpha \to 0 \text{ @ horizon}$$

$$\alpha \to 1 \text{ @ infinity}$$

$$\mathbf{B}_p = -\frac{e_\phi \times \nabla\Psi}{2\pi\varpi}, \quad \varpi : \text{ distance from rotation axis.}$$

If $\rho \neq \rho_{\mathrm{GJ}}$ in any region, $E_{\parallel} \neq 0$ arises around it.

$\rho_{\mathrm{GJ}}=0$ near $\omega=\Omega_{\mathrm{F}}$. Thus, pulsar-like ‘null charge surface’ appears near the horizon. A vacuum gap can arise there.

§ 3 Method: Basic equations

KH + (2006a,b)

To solve $E_\parallel$, we must solve the **Poisson eq.**

Near the horizon ($\Delta \equiv r^2 - 2Mr + a^2 \ll M^2$), it becomes

$$-\left(\frac{r^2+a^2}{\Delta}\right)^2 \frac{\partial^2 \Phi}{\partial r_*^2} + \frac{2(r-r_g)(r^2+a^2)}{\Delta^2}\frac{\partial \Phi}{\partial r_*}$$

$$-\frac{\Sigma}{\Delta \sin\theta}\frac{\partial}{\partial \theta}\left(\frac{\sin\theta}{\Sigma}\frac{\partial \Phi}{\partial \theta}\right) = \left(\frac{\Sigma}{r^2+a^2}\right)^2 (n_+ - n_- - n_{\mathrm{GJ}})$$

where $E_\parallel \equiv -(\mathbf{B}\bullet\nabla)\Phi / B$ and $\Sigma \equiv r^2 + a^2 \cos^2\theta$.

The tortoise coordinate r_* is related to the polar r by

$$\frac{dr_*}{dr} = \frac{r^2+a^2}{\Delta}$$

§ 3 Method: Basic equations

KH + (2006a,b)

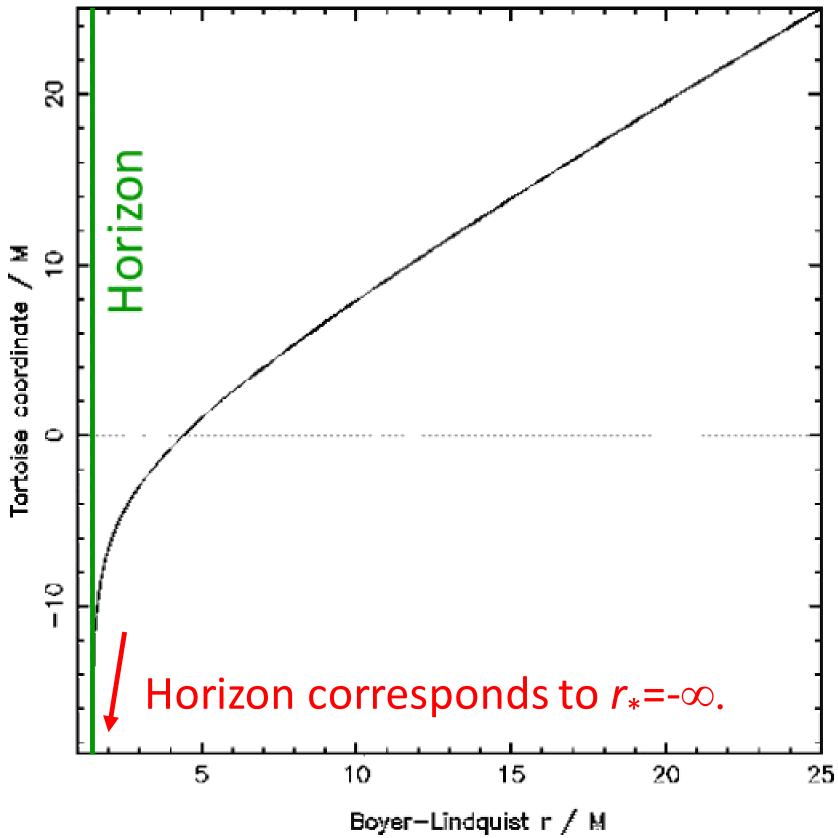

Tortoise coordinate vs. Boyer-Lindquist *r* coordinate

The tortoise coordinate r_* is related to the polar r by

$$\frac{dr_*}{dr} = \frac{r^2 + a^2}{\Delta}$$

§ 3 Method: Basic eqs.

KH + (2006b)

Poisson eq.:

$$-\left(\frac{r^2+a^2}{\Delta}\right)^2\frac{\partial^2\Phi}{\partial r_*{}^2}+\frac{2(r-r_g)(r^2+a^2)}{\Delta^2}\frac{\partial\Phi}{\partial r_*}$$

$$-\frac{\Sigma}{\Delta\sin\theta}\frac{\partial}{\partial\theta}\left(\frac{\sin\theta}{\Sigma}\frac{\partial\Phi}{\partial\theta}\right)=\left(\frac{\Sigma}{r^2+a^2}\right)^2(n_+-n_--n_{\mathrm{GJ}})$$

Instead of solving the ***e***$^{\pm}$ **Boltzmann eqs**., we assume that the Lorentz factors are saturated at the curvature- or ICS-limited value, whichever smaller, $\gamma=\min(\gamma_{\mathrm{curv}},\gamma_{\mathrm{ICS}})$. Solve n_+ & n_- from the pair production at each position, using the γ-ray specific intensity solved from the R. T. E.

Radiative transfer eq.: $$\frac{dI_\nu}{dl}=-\alpha_\nu I_\nu+j_\nu$$

§ 4 Results: the case of stellar-mass BHs

Consider a stellar-mass BH, $M=10M_{\odot}$, assuming $B=B_{eq}$.

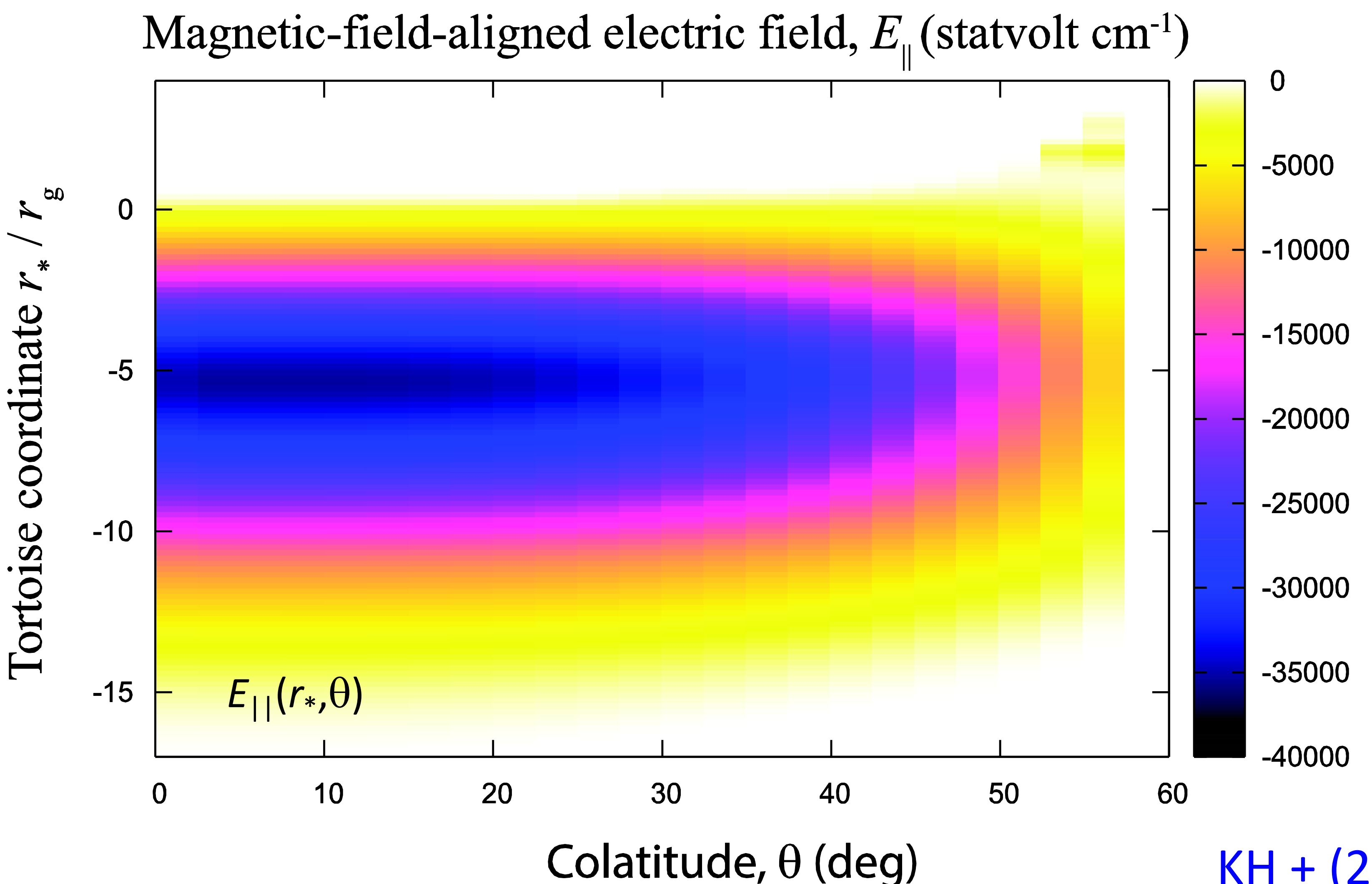

KH + (2016b)

§ 4 Results: stellar-mass BHs

M=10$M_\odot$, B=B_{eq}.

Slice $E_\parallel(r_*, \theta)$ at six θ's.

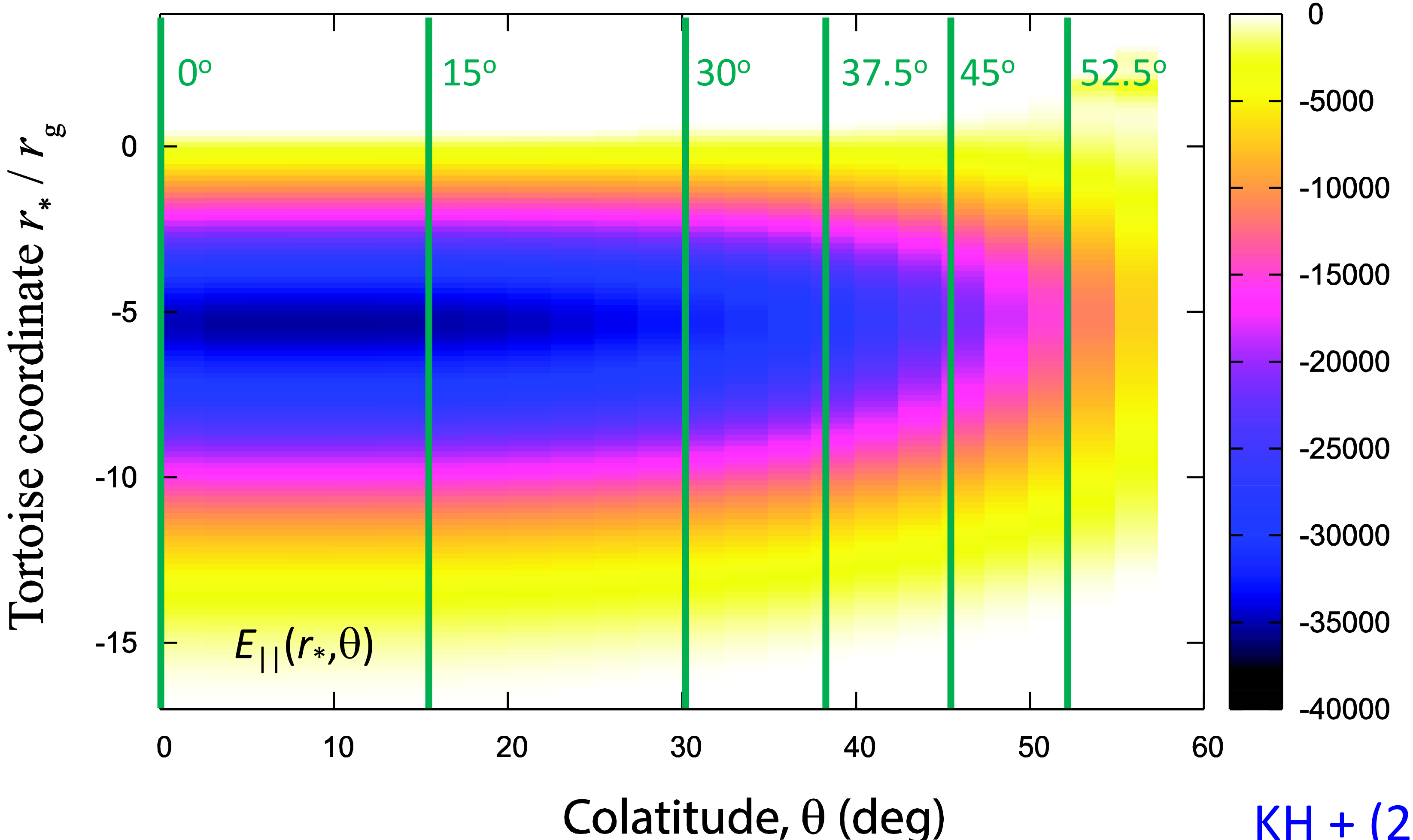

KH + (2016b)

§ 4 Results: stellar-mass BHs

$M=10M_{\odot}$, $B=B_{eq}$

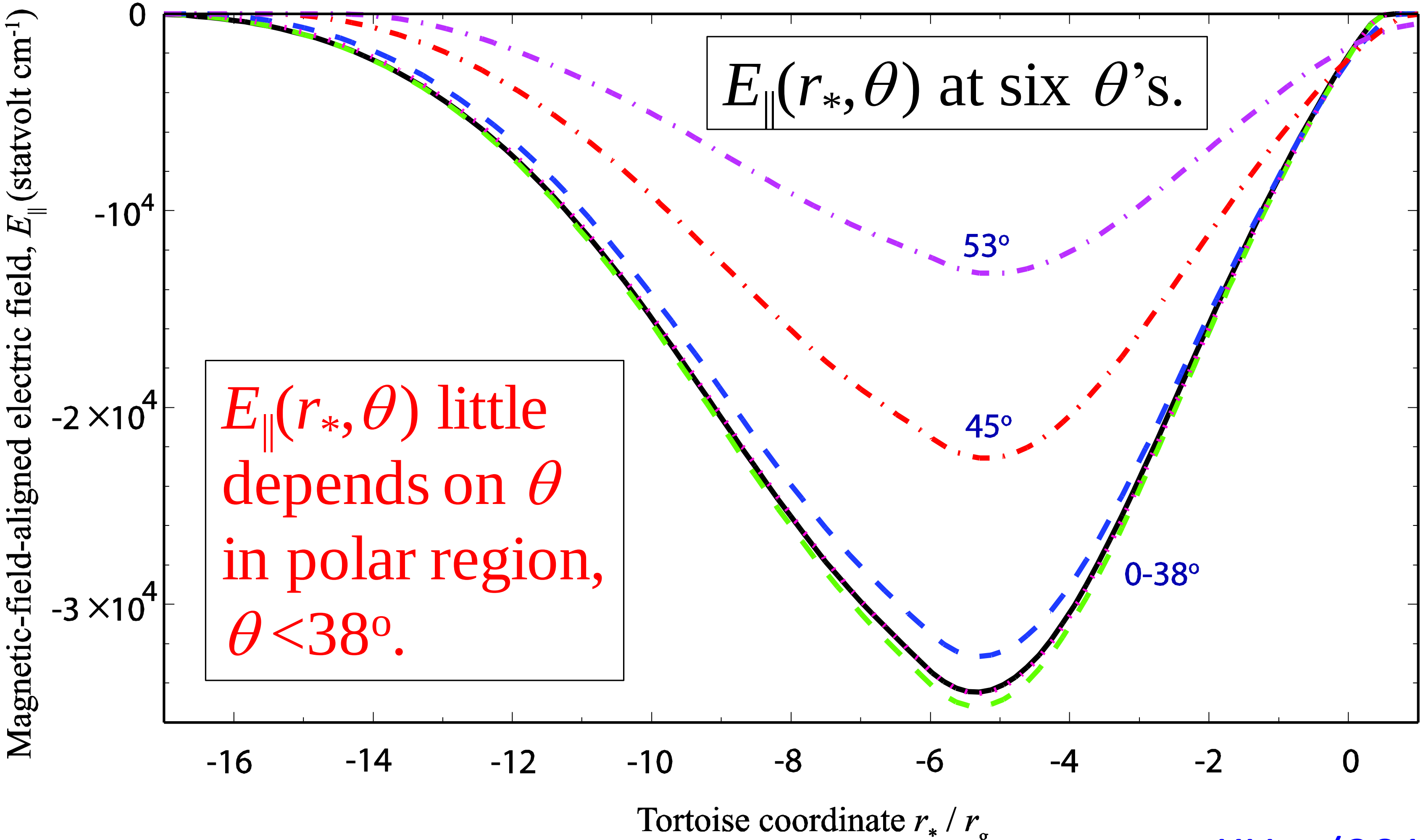

KH + (2016b)

§ 4 Results: stellar-mass BHs

M=10$M_{\odot}$, B=B_{eq}

γ-ray spectra

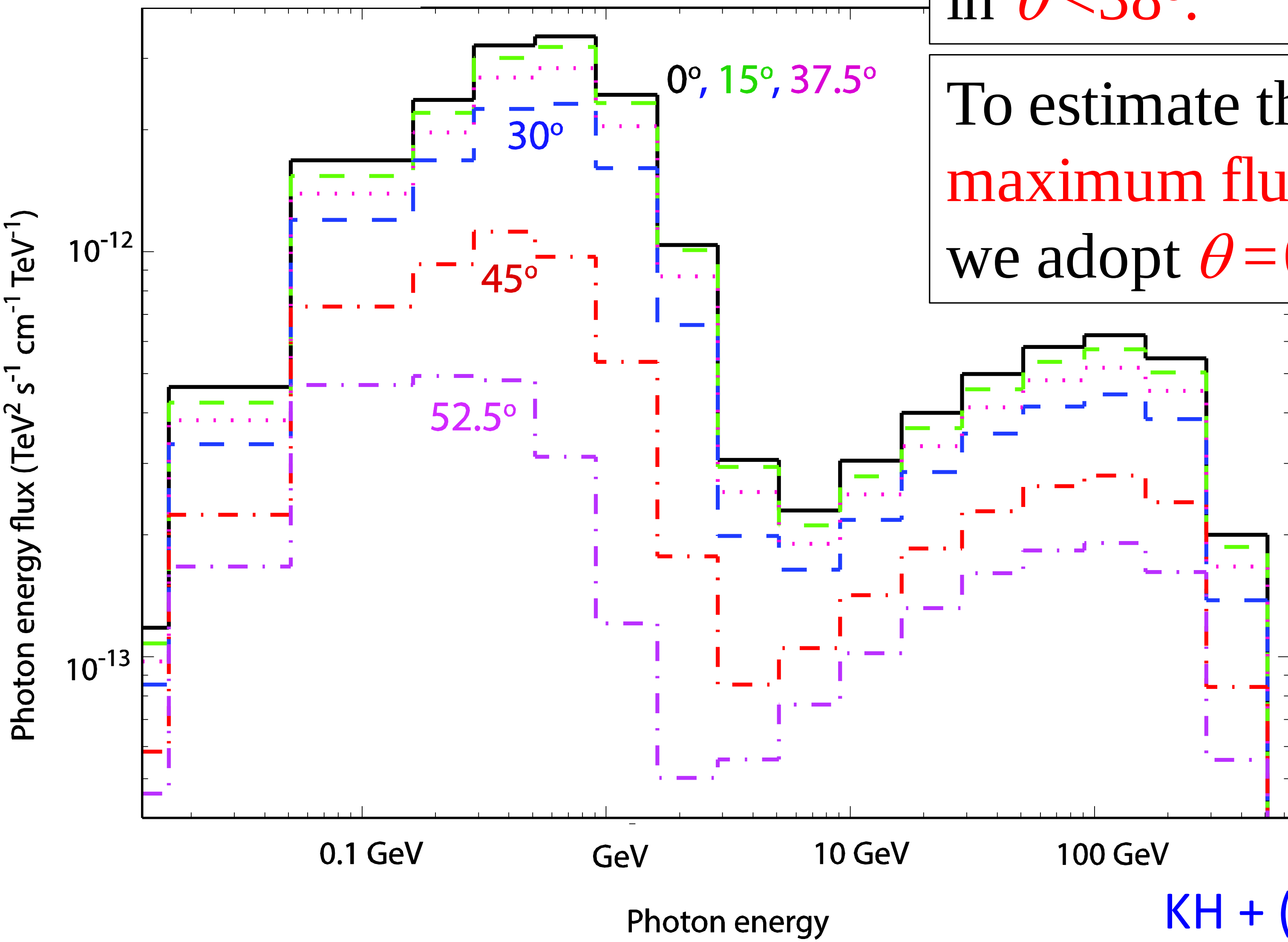

SED little changes in θ<38°.

To estimate the maximum flux, we adopt θ=0°.

KH + (2016b)

§ 4 Results: stellar-mass BHs

$M=10M_\odot$, $B=B_{eq}$; Lepton densities per **B** flux @ $\theta=0^o$

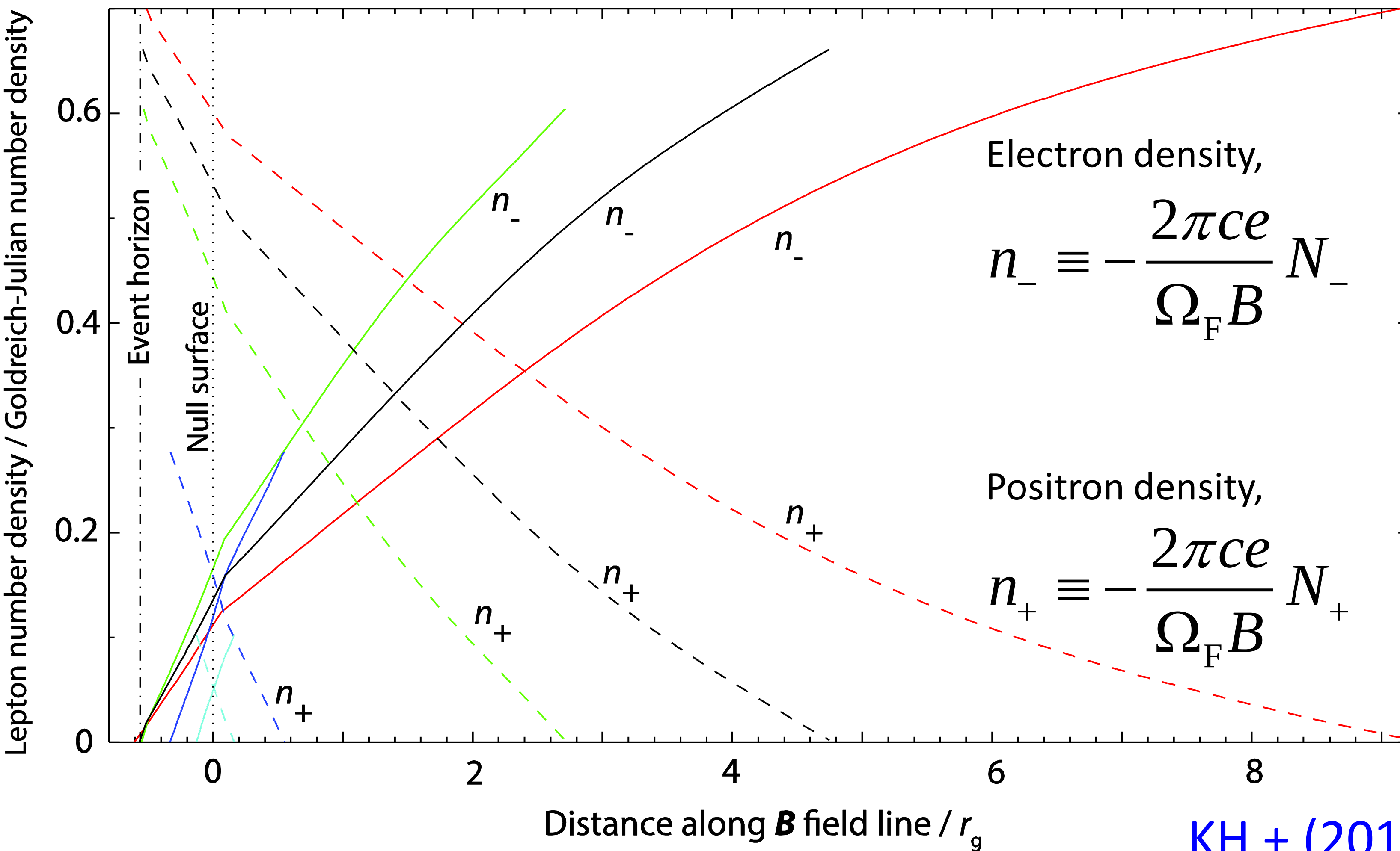

KH + (2016b)

§ 4 Results: stellar-mass BHs

$M=10M_\odot$, $B=B_{eq}$; $E_\parallel(r-r_0,\theta)$ @ $\theta=0^o$

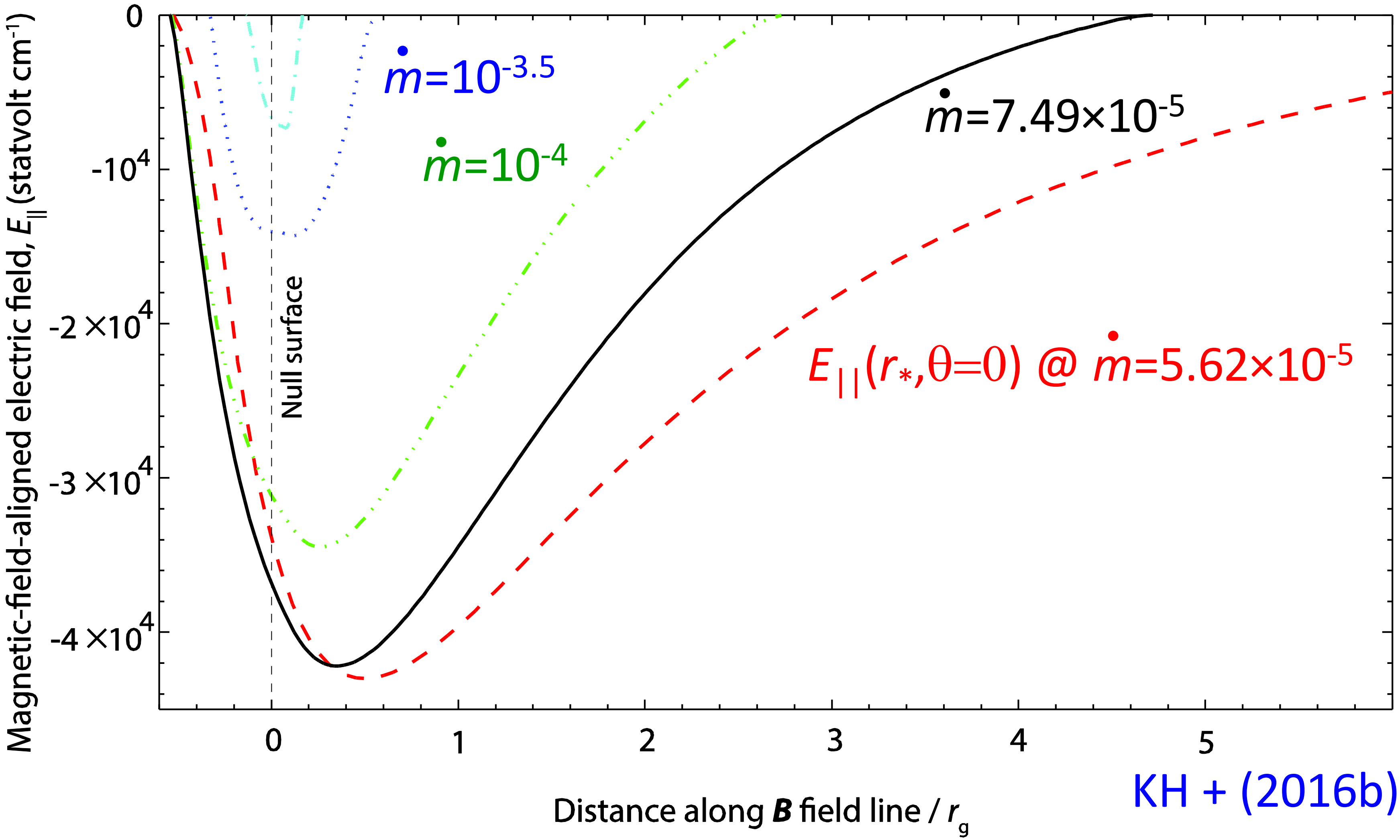

KH + (2016b)

§ 4 Results: stellar-mass BHs

M=10$M_{\odot}$, B=B_{eq}; outer & inner boundaries @ θ=0°

Gap width increases with decreasing accretion rate.

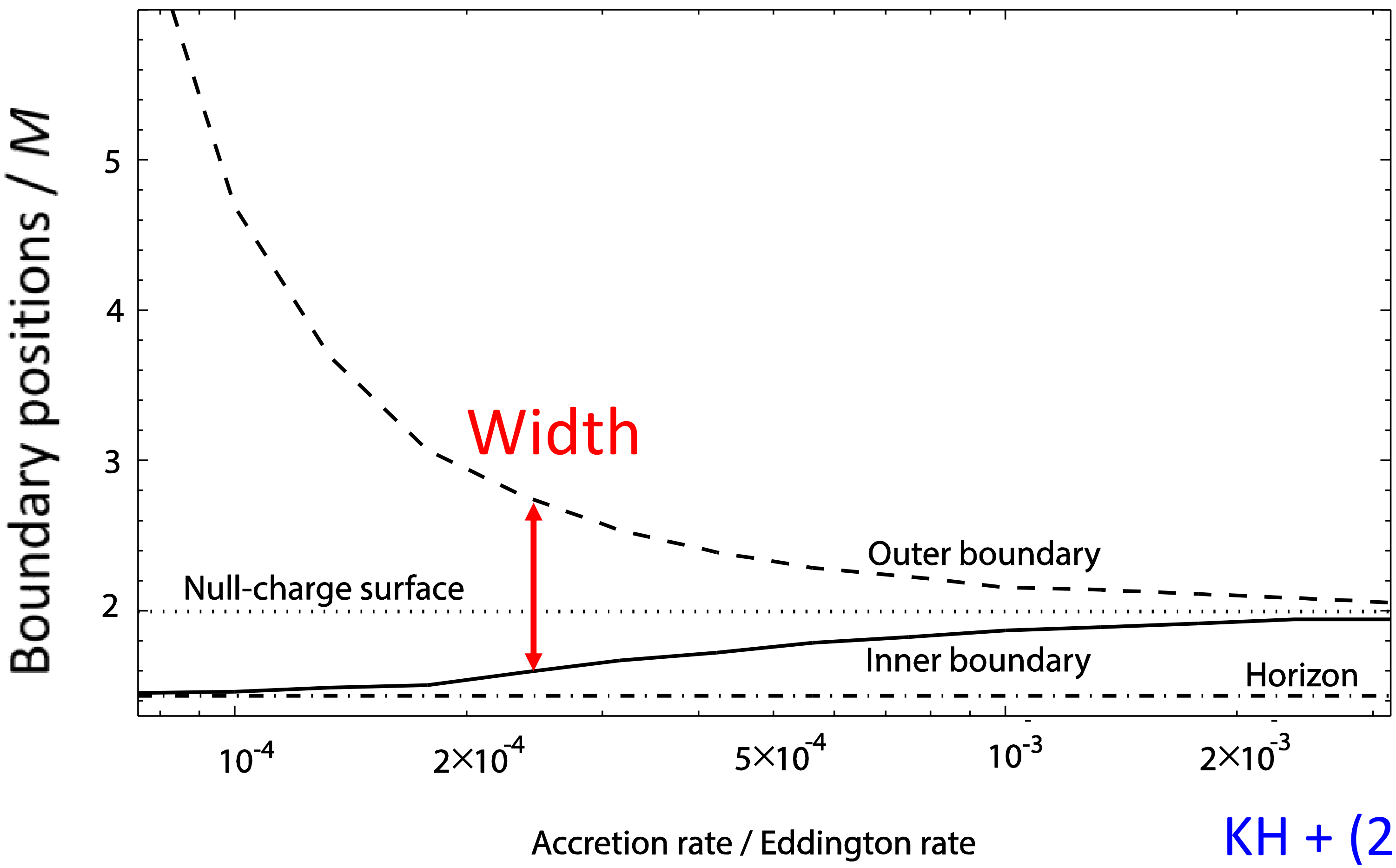

KH + (2016b)

§ 4 Results: stellar-mass BHs

M=$10M_{\odot}$, B=B_{eq}; SED vs. current density, j (θ=0).
j~0.7 optimizes HE & VHE fluxes.

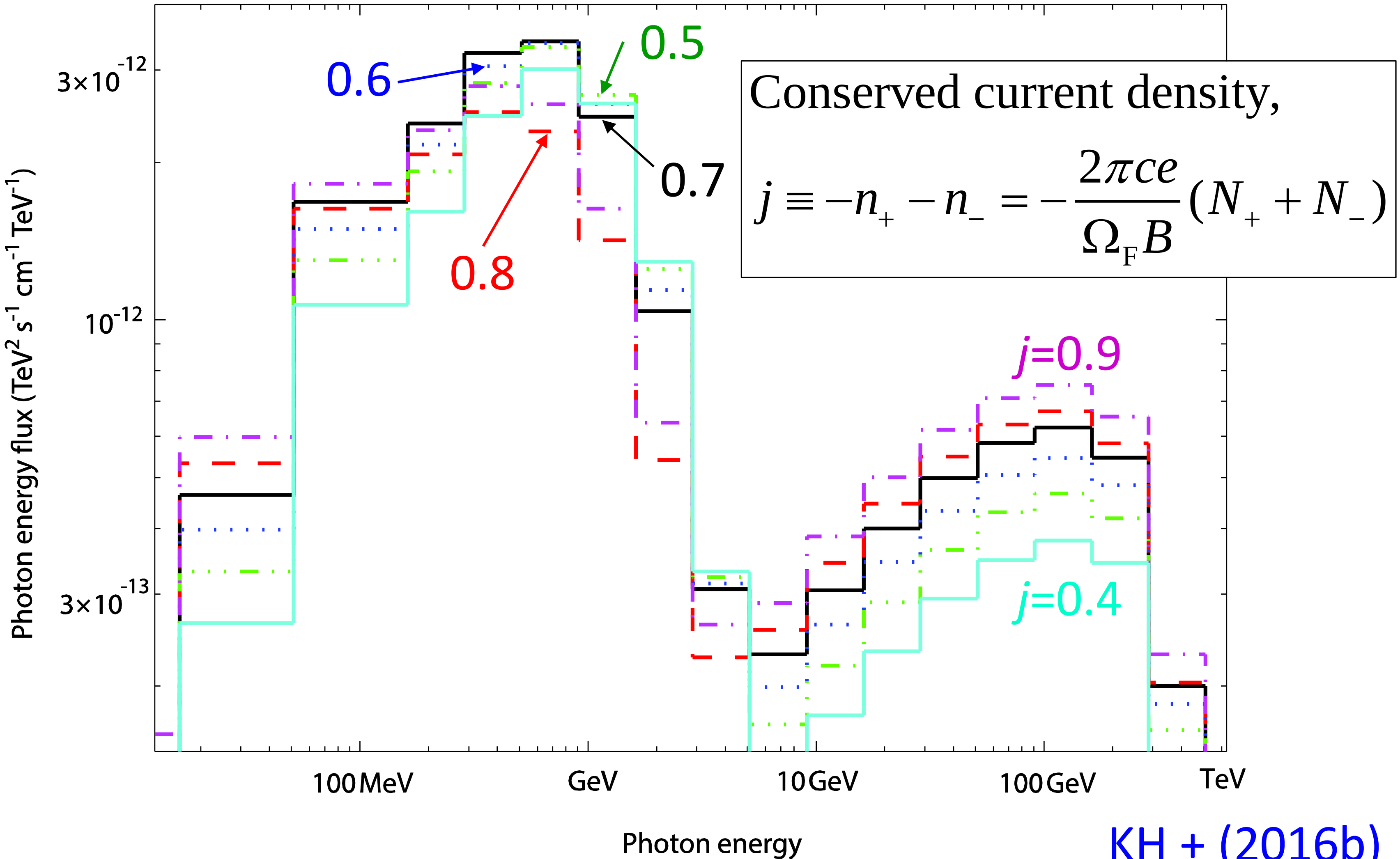

KH + (2016b)

§ 4 Results: stellar-mass BHs

M=10$M_\odot$, B=B_{eq}; SEDs @ five discrete $\dot{m}$ (θ=0°)

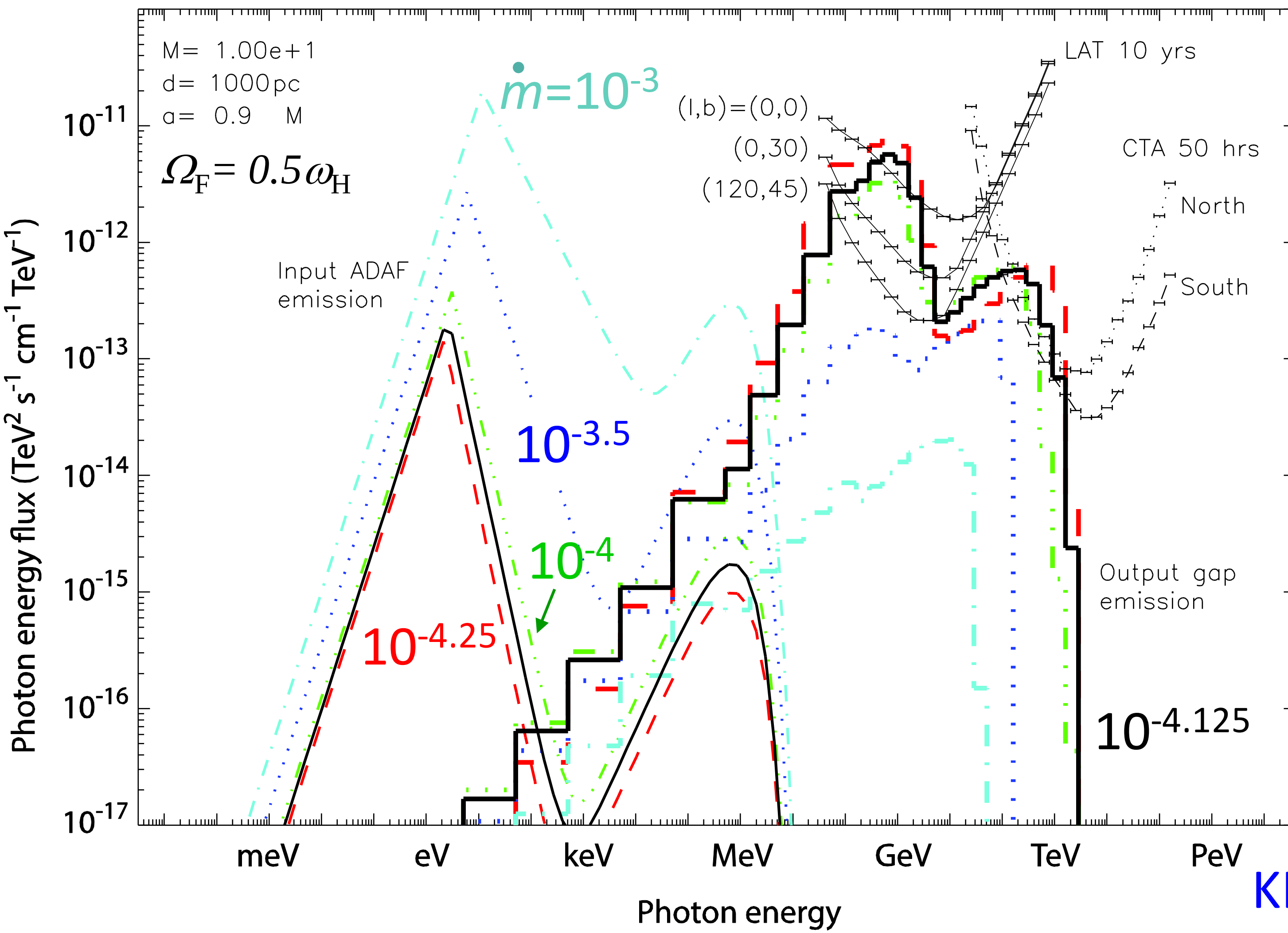

KH + (2016b)

§ 4 Results: stellar-mass BHs

M=$10M_{\odot}$, B=B_{eq}; SEDs @ five discrete $\dot{m}$ (θ=0°)

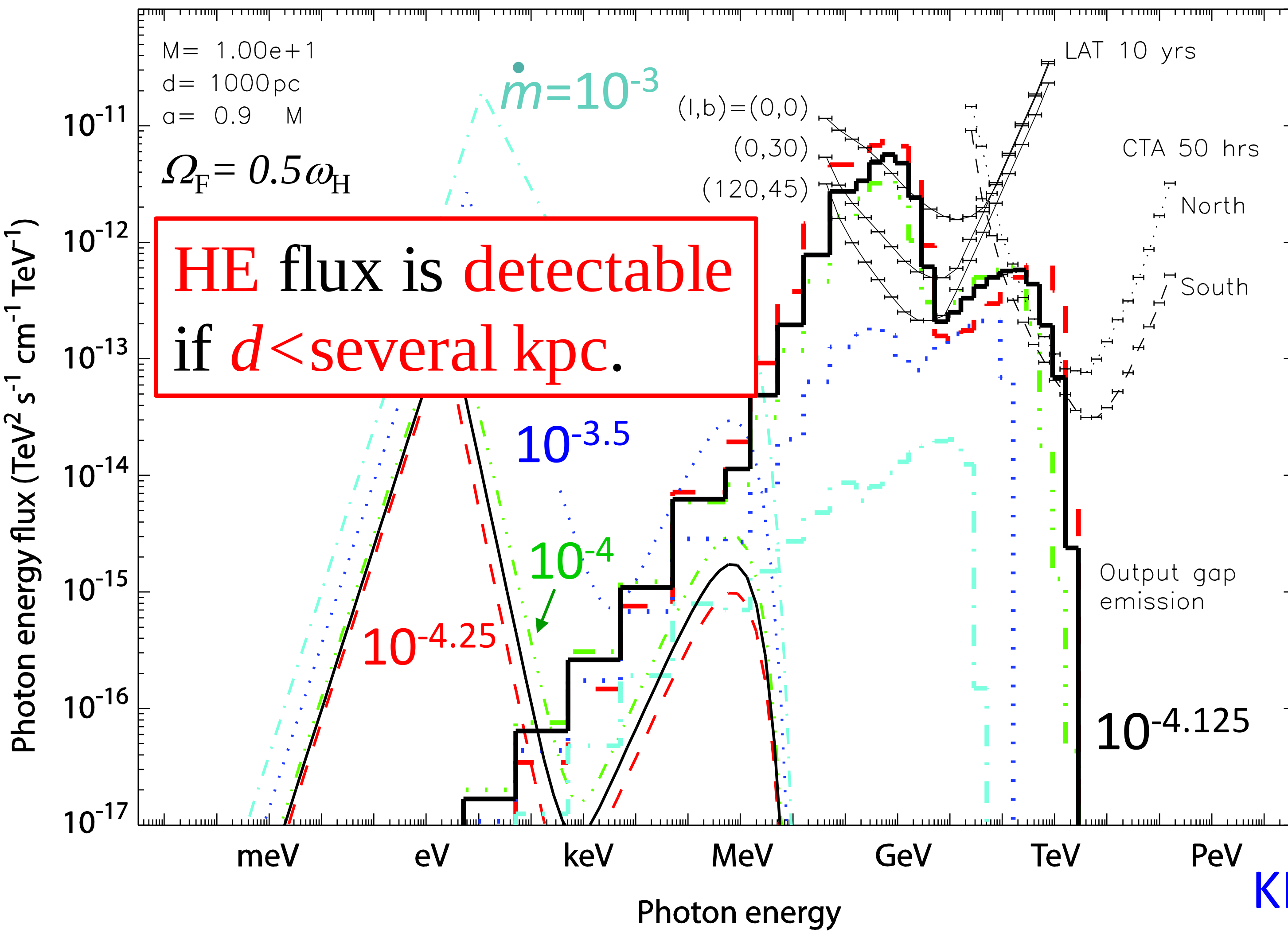

KH + (2016b)

§ 4 Results: stellar-mass BHs

$M=10M_{\odot}$, $B=B_{eq}$; Emission components ($\theta=0^{o}$)

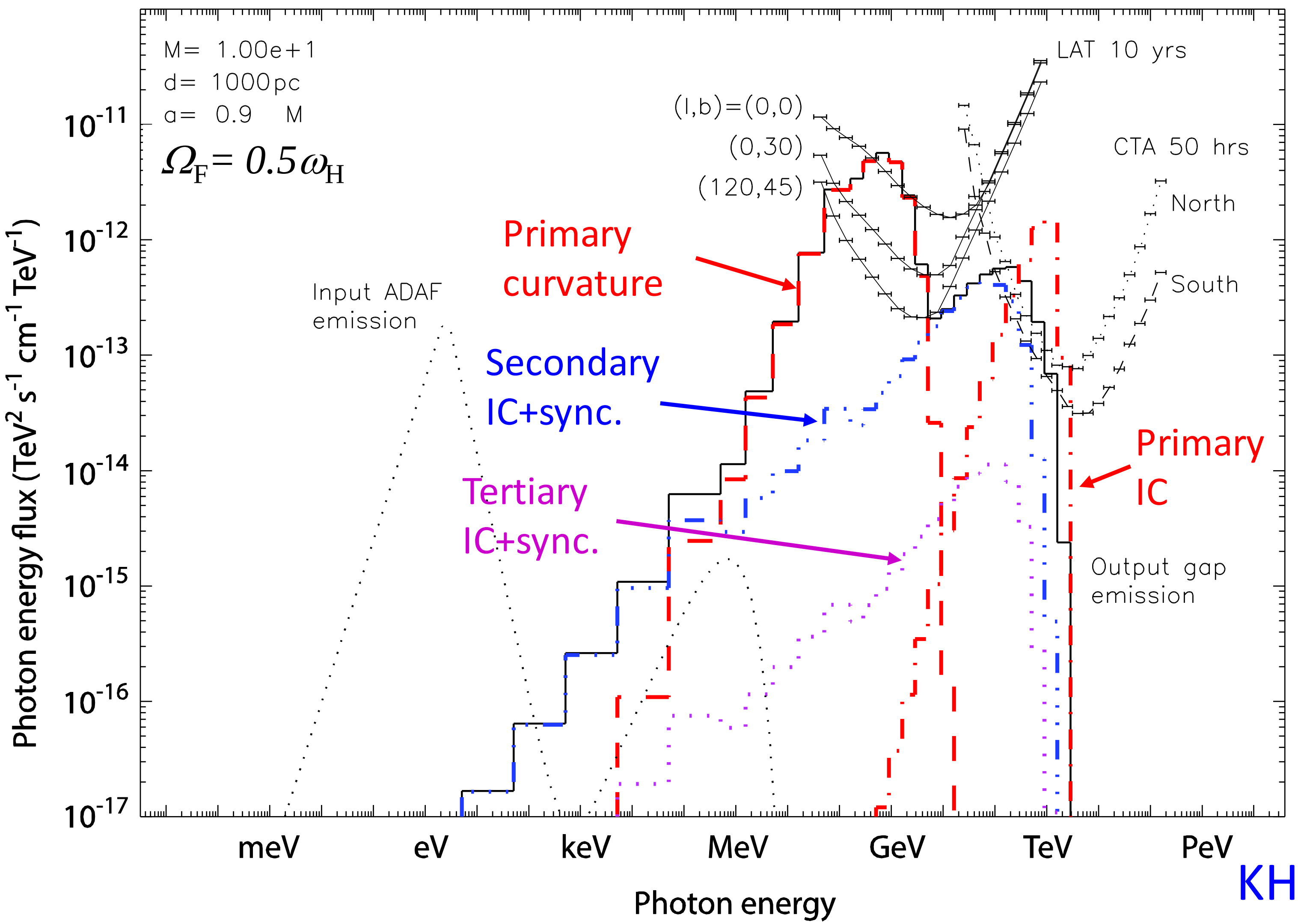

KH + (2016b)

§ 4 Results: stellar-mass BHs

$M=10M_{\odot}$, $B=B_{eq}$; Optical depths ($\theta=0^{\circ}$)

Test photons are emitted from inner BD.

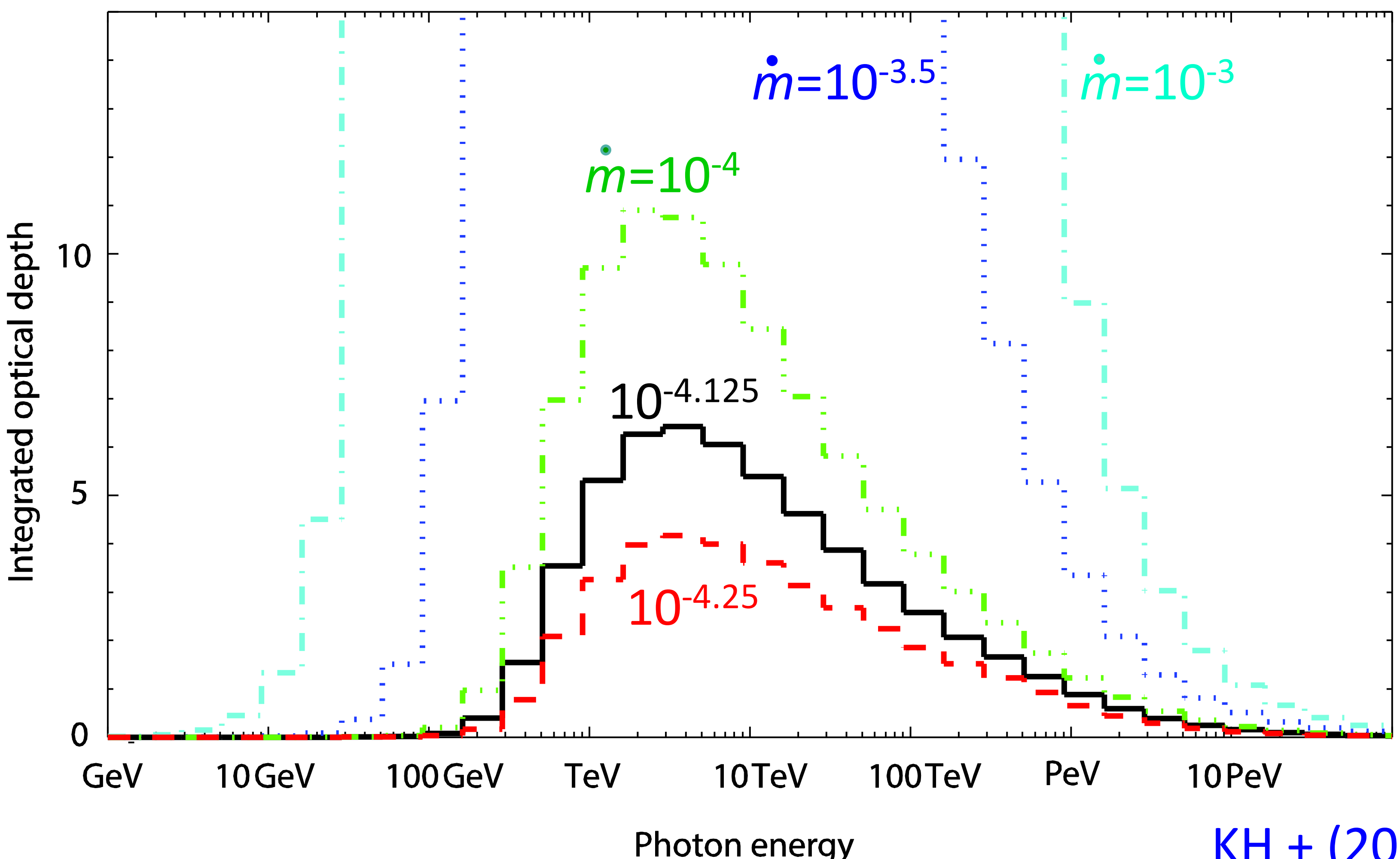

KH + (2016b)

§ 4 Results: stellar-mass BHs

$M=10M_{\odot}$, $B=B_{eq}$; Curvature vs. IC luminosity ($\theta=0^{o}$)

Curvature » IC @ $\dot{m}<2\times10^{-4}$.

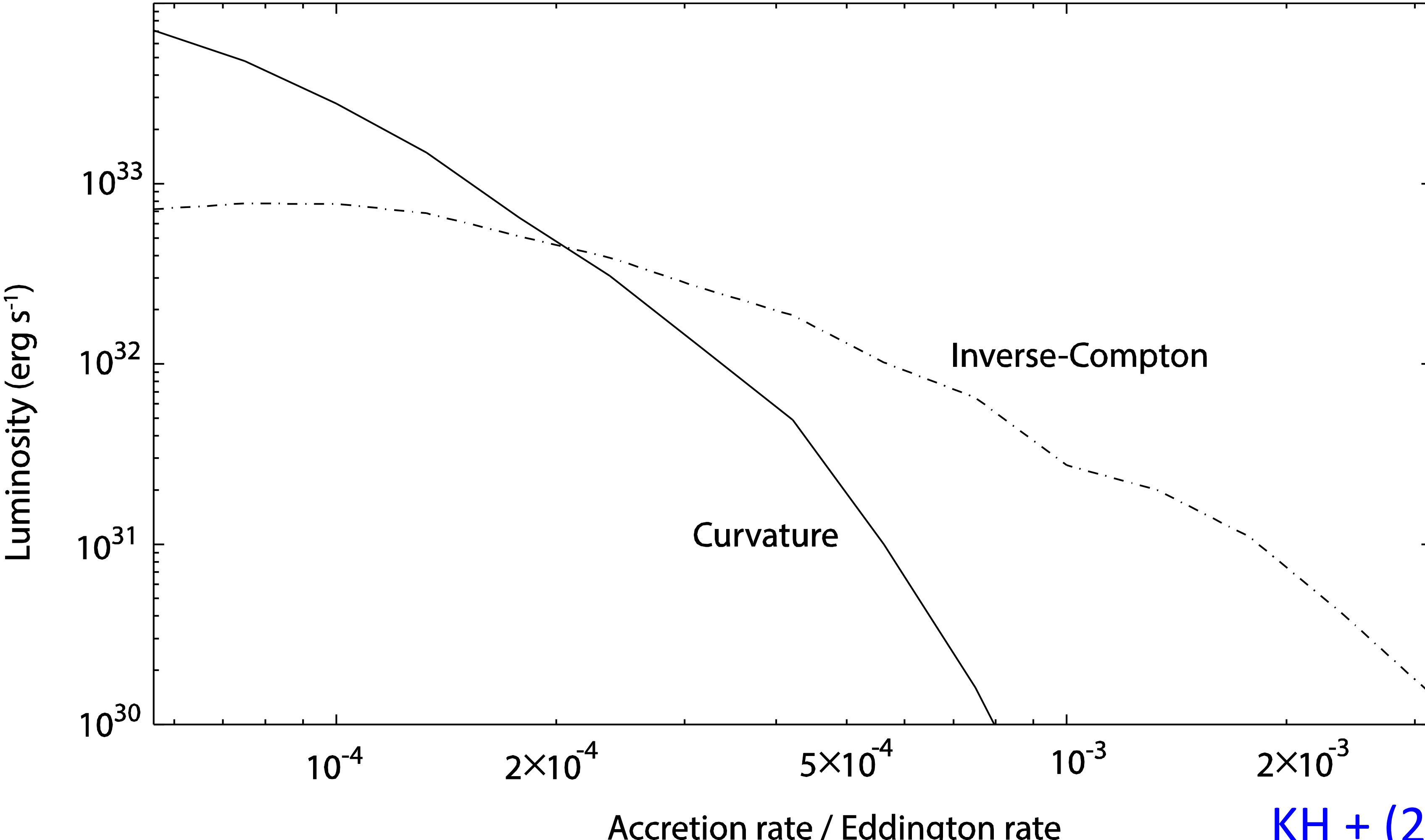

KH + (2016b)

§ 4 Results: stellar-mass BHs

M=*10M*$_\odot$, *B*=*B*$_{eq}$; SED @ slower BH spin, *a=0.5* (θ=0).
HE & VHE fluxes decreases cf. *a=0.9*.

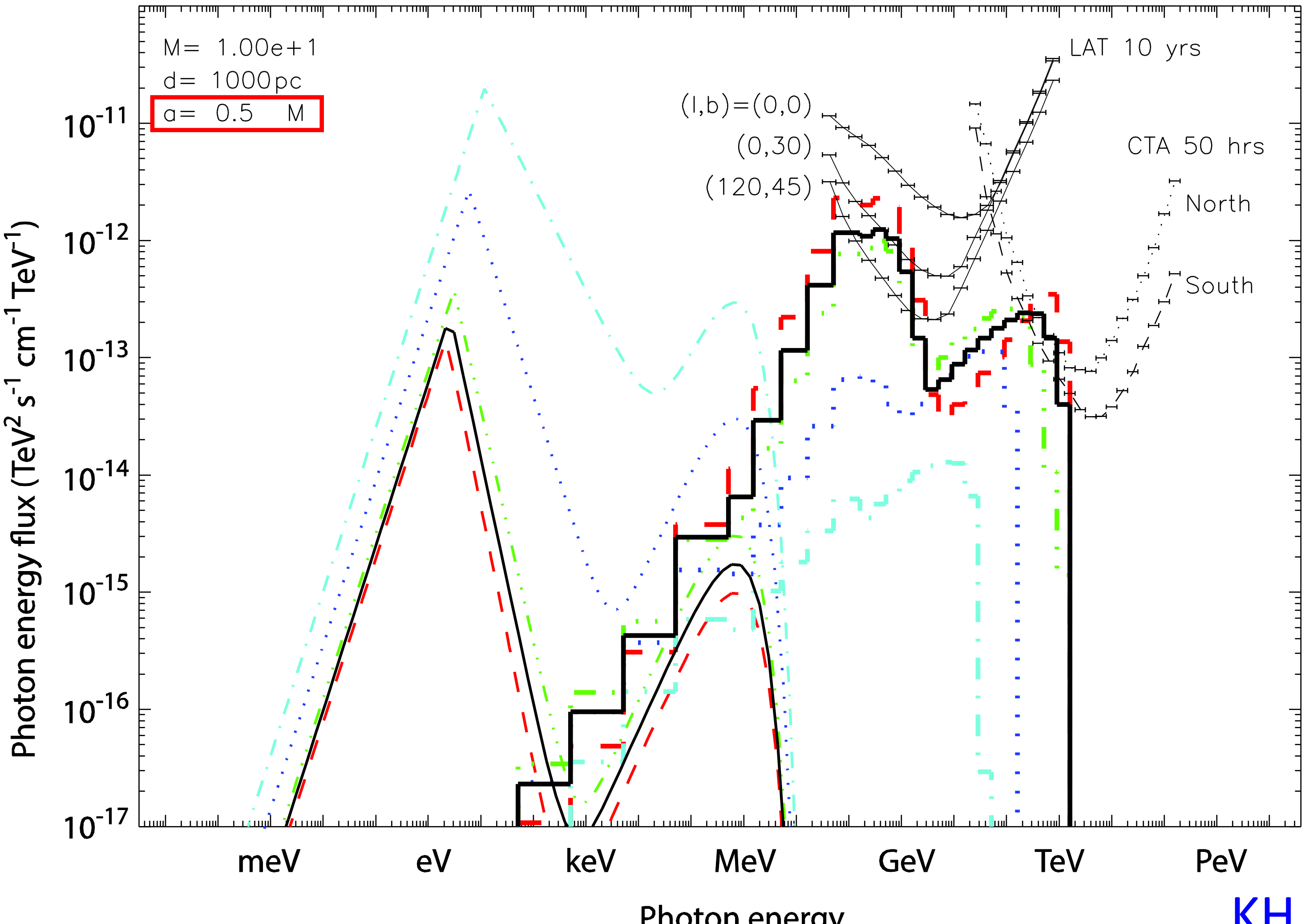

KH + (2016b)

§ 4 Results: stellar-mass BHs

$M=10M_{\odot}$, $B=B_{eq}$; SED @ extreme spin, $a=0.998$ ($\theta=0$).

HE & VHE fluxes increases w/ a.

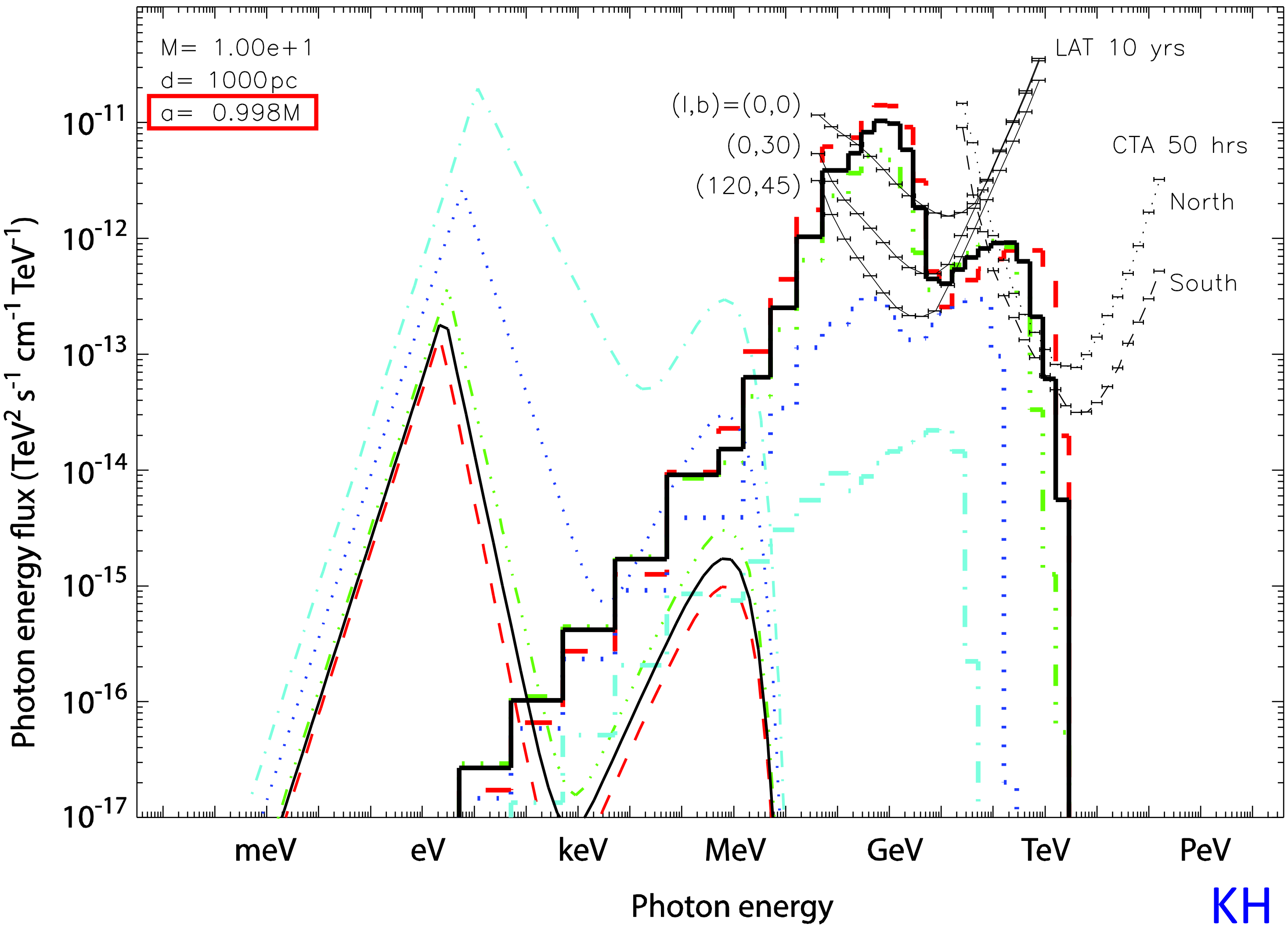

KH + (2016b)

§ 4 Results: stellar-mass BHs

$M=10M_{\odot}$, $B=B_{eq}$; SED @ extreme spin, $a=0.998$ ($\theta=0$).
HE & VHE fluxes increases w/ a.

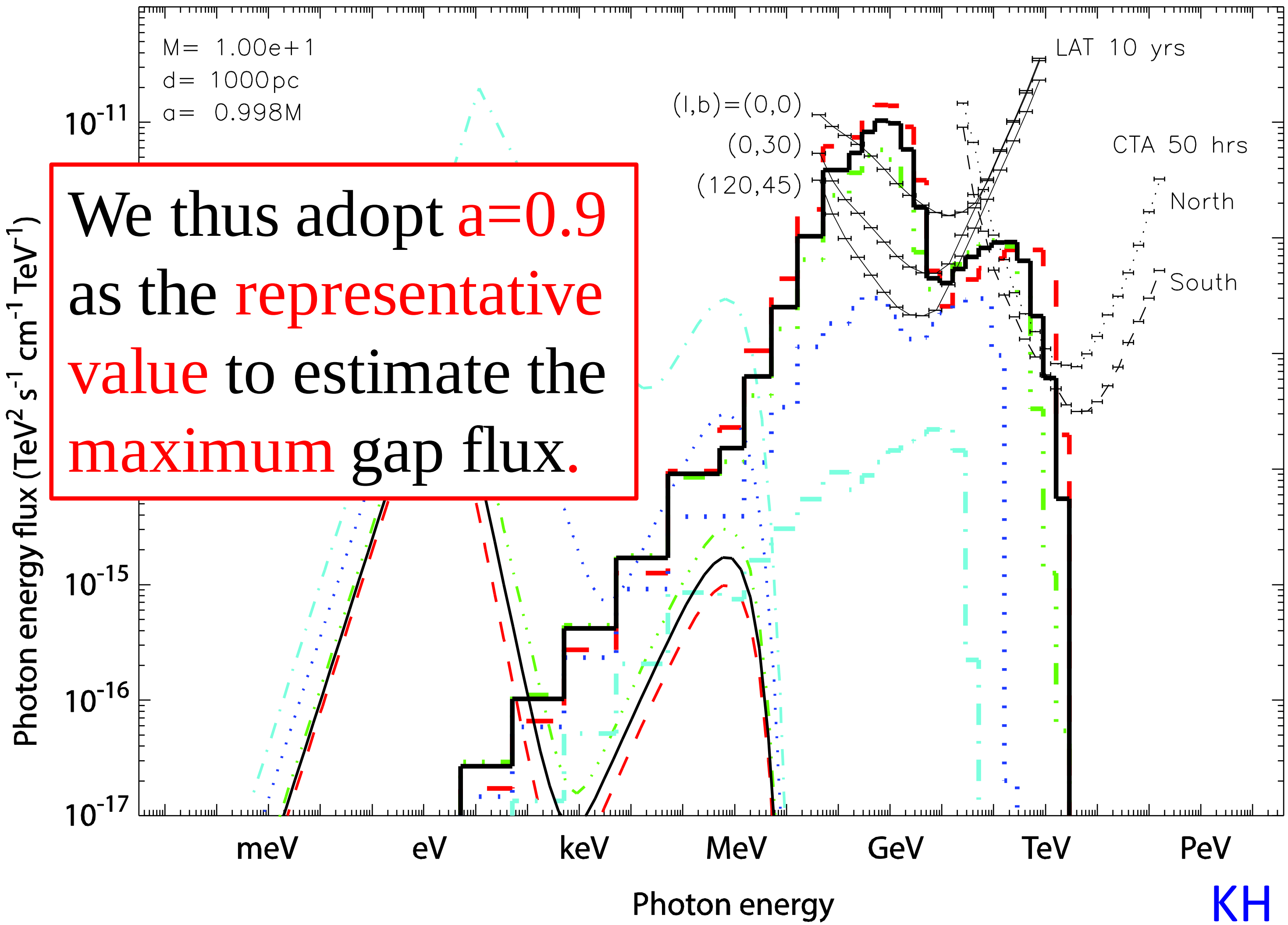

We thus adopt a=0.9 as the representative value to estimate the maximum gap flux.

KH + (2016b)

§ 4 Results: stellar-mass BHs

M=10*M*$_{\odot}$, *B*=*B*$_{eq}$; SED @ slower **B** rotation (θ=0).

HE & VHE fluxes max. @ Ω_F~0.5ω_H.

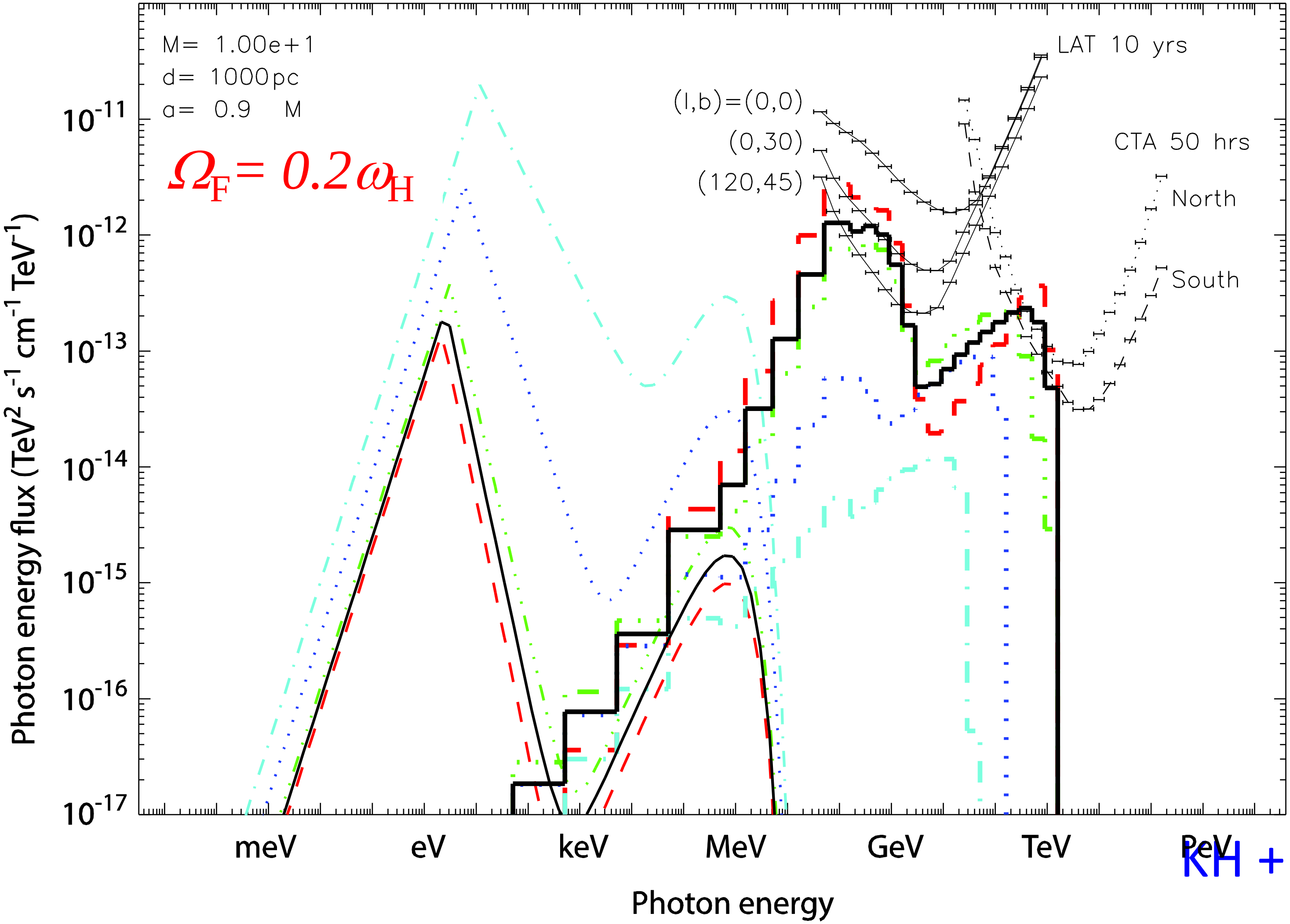

KH + (2016b)

§ 4 Results: stellar-mass BHs

$M=10M_{\odot}$, $B=B_{eq}$; Cascaded pair density » GJ @ $^{\forall}\dot{m}$.

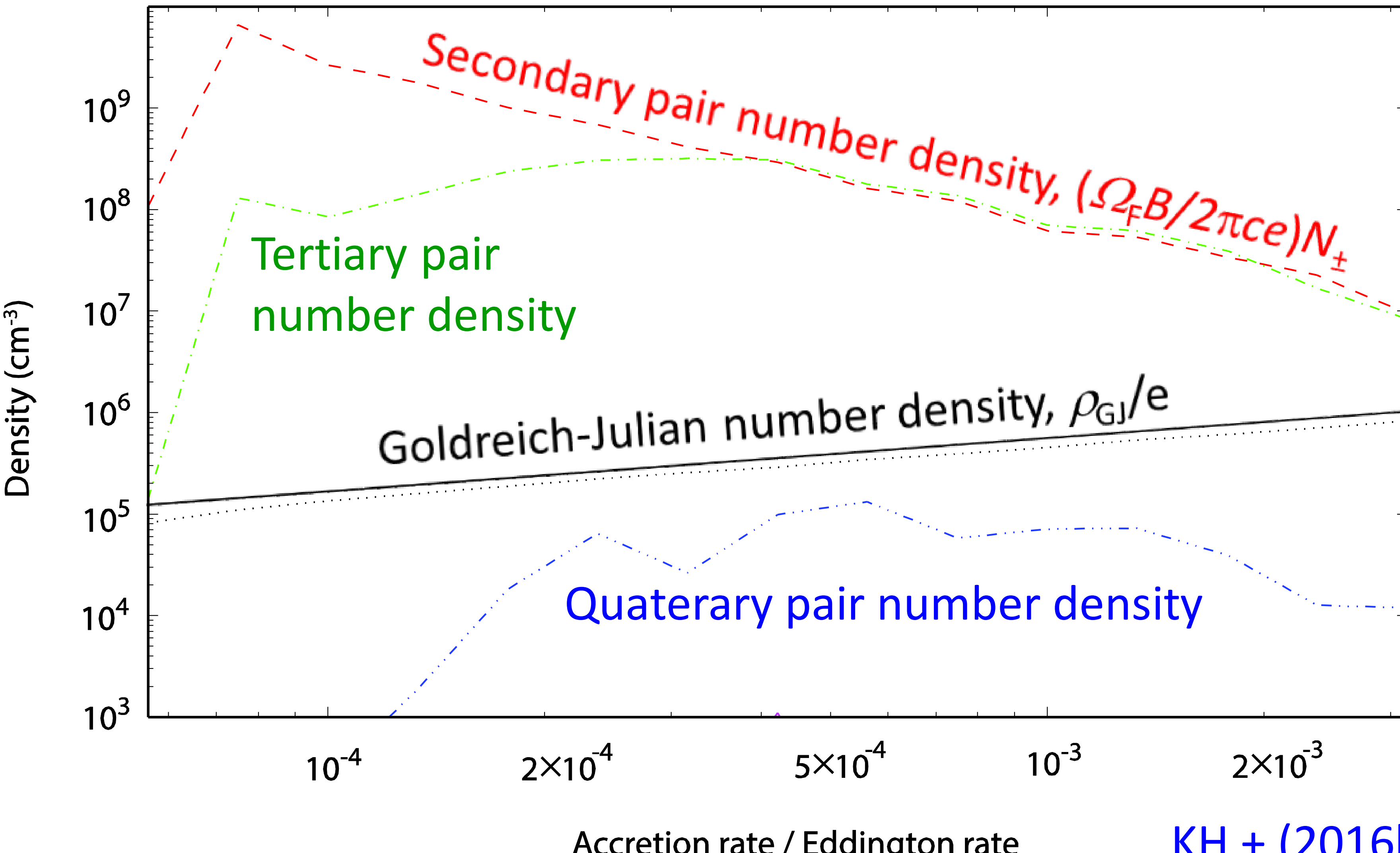

KH + (2016b)

§ 5 Results: super-massive BHs

For SMBH, $M=10^9 M_\odot$, $B=B_{eq}$; SED @ five $\dot{m}$'s.

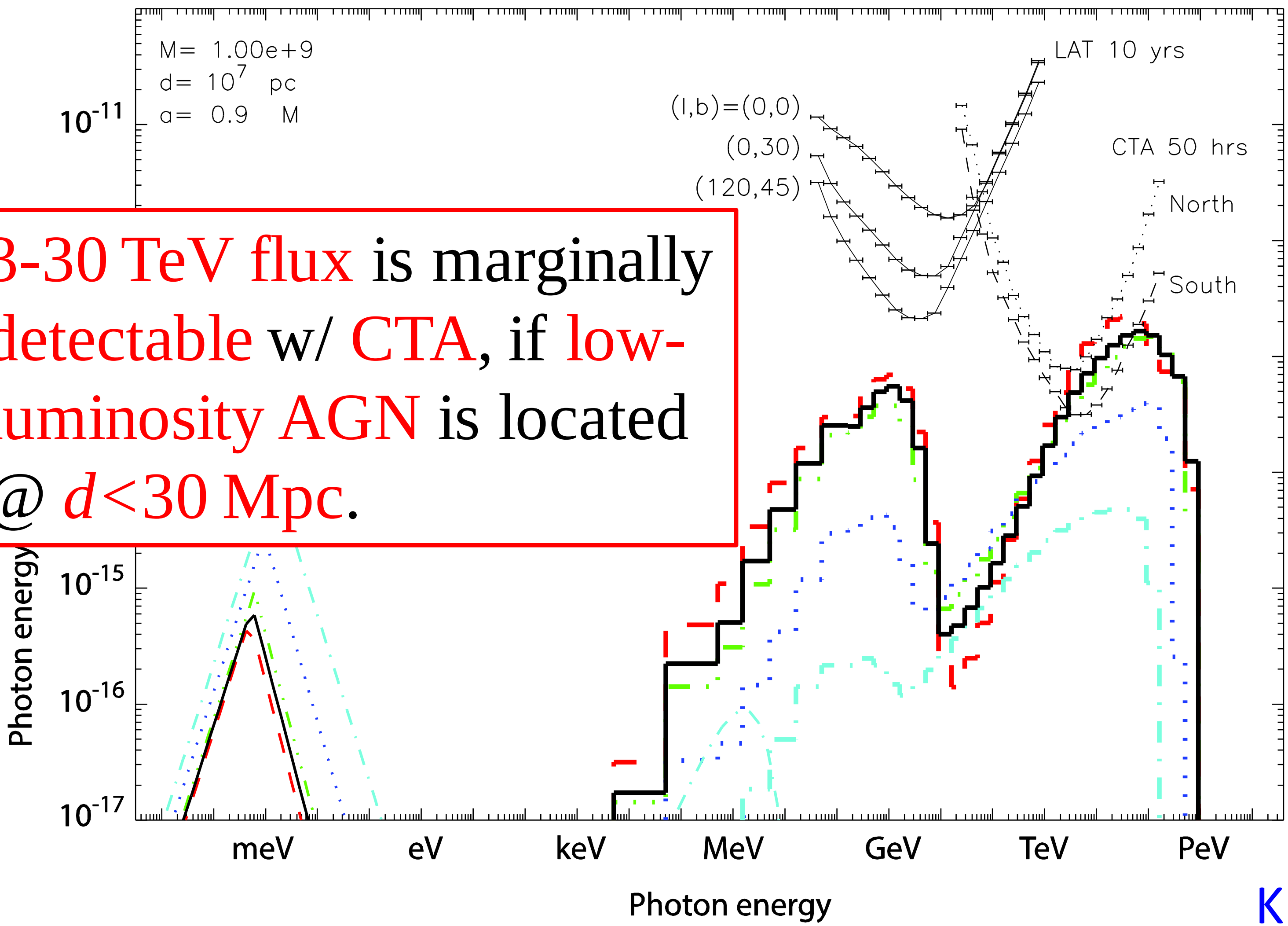

3-30 TeV flux is marginally detectable w/ CTA, if low-luminosity AGN is located @ d<30 Mpc.

KH + (2016b)

§ 5 Results: SMBHs

$M=10^9 M_\odot$, $B=B_{eq}$; IC » Curvature for super-massive BHs.

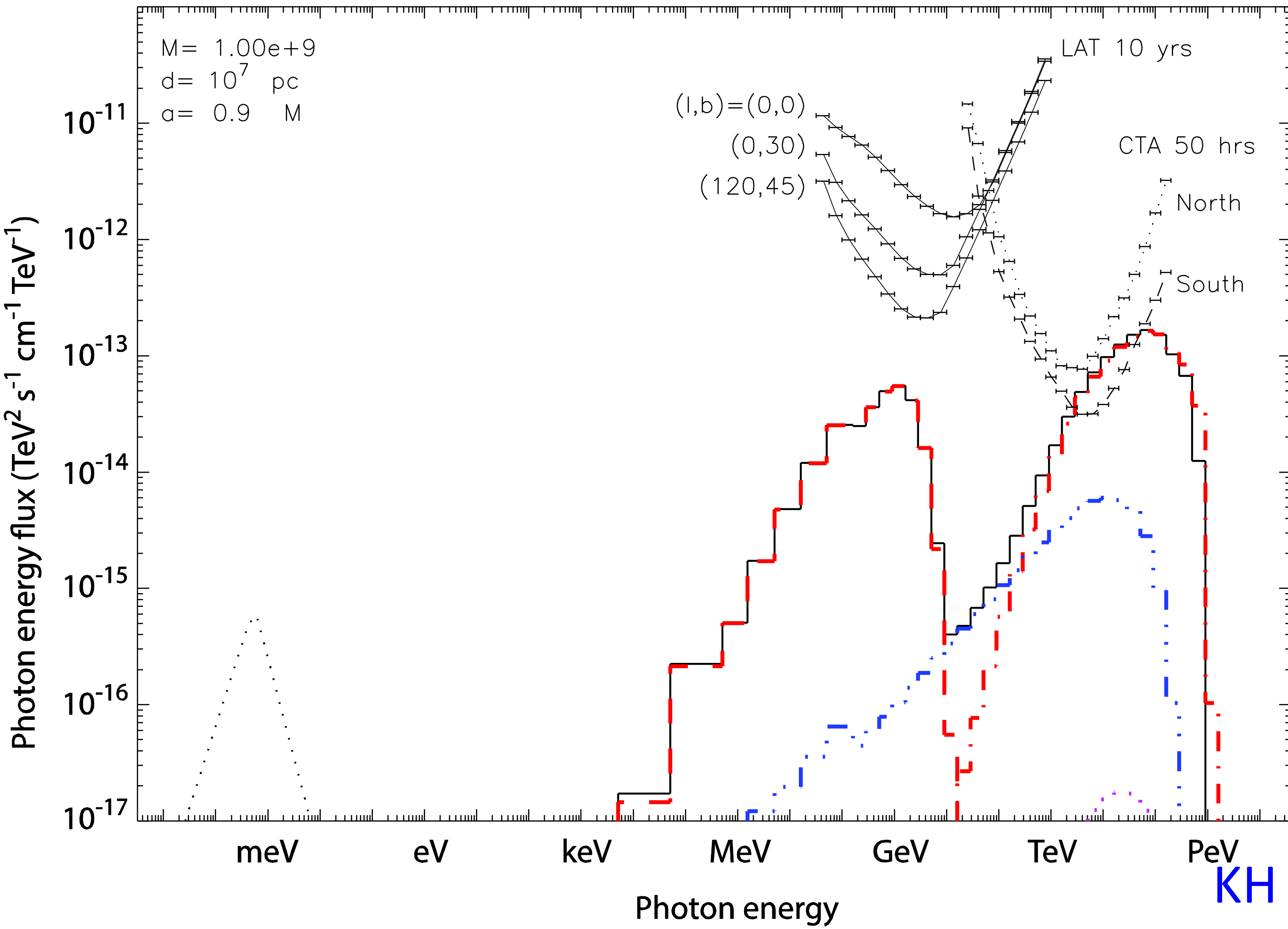

KH + (2016b)

§ 5 Results: SMBHs

$M = 10^9 M_\odot$, $B = B_{eq}$; IC » Curvature @ $^\forall \dot{m}$.

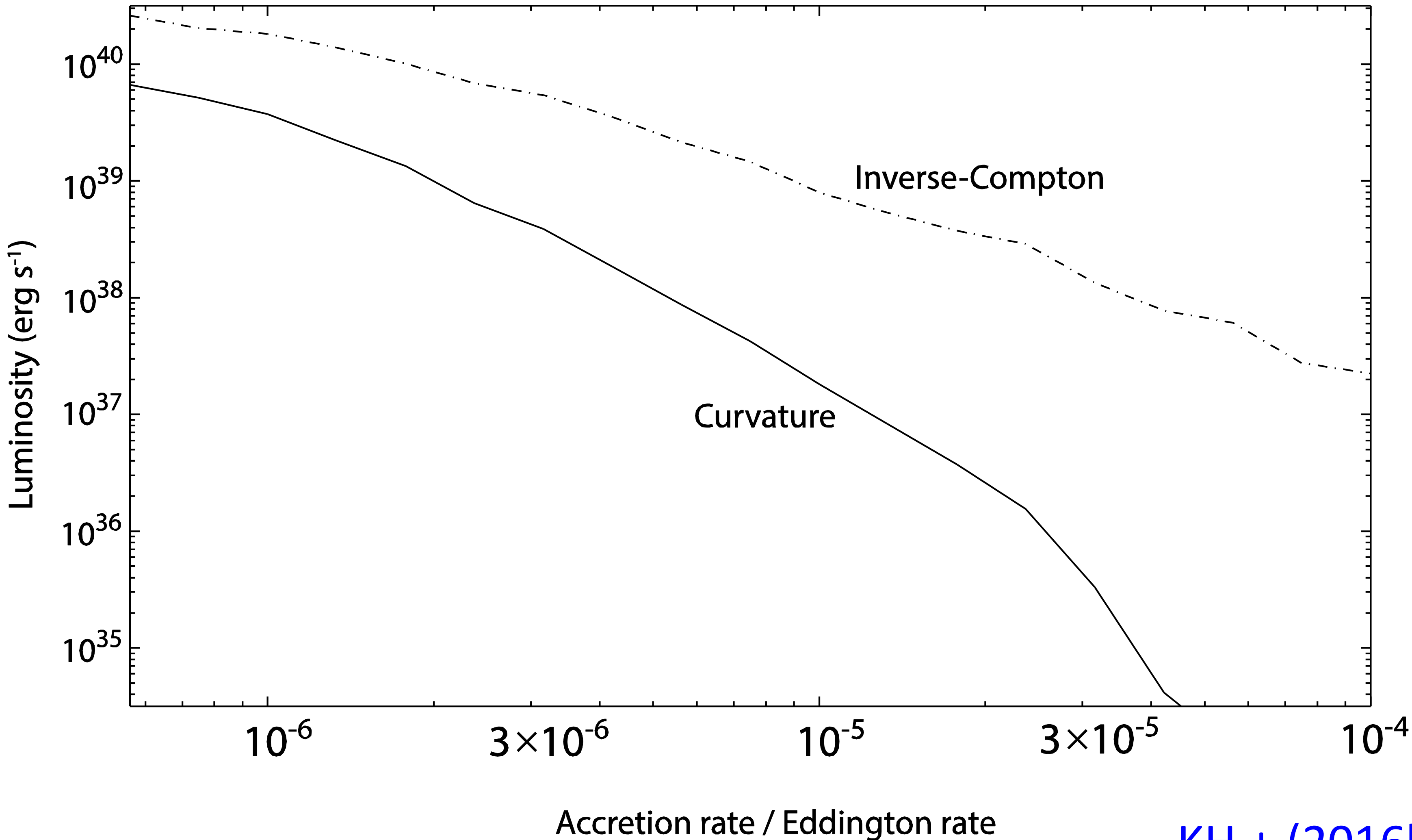

KH + (2016b)

§ 5 Results: SMBHs

$M = 10^9 M_{\odot}$, $B = B_{\mathrm{eq}}$; Cascaded pair density » GJ @ $^{\forall}\dot{m}$.

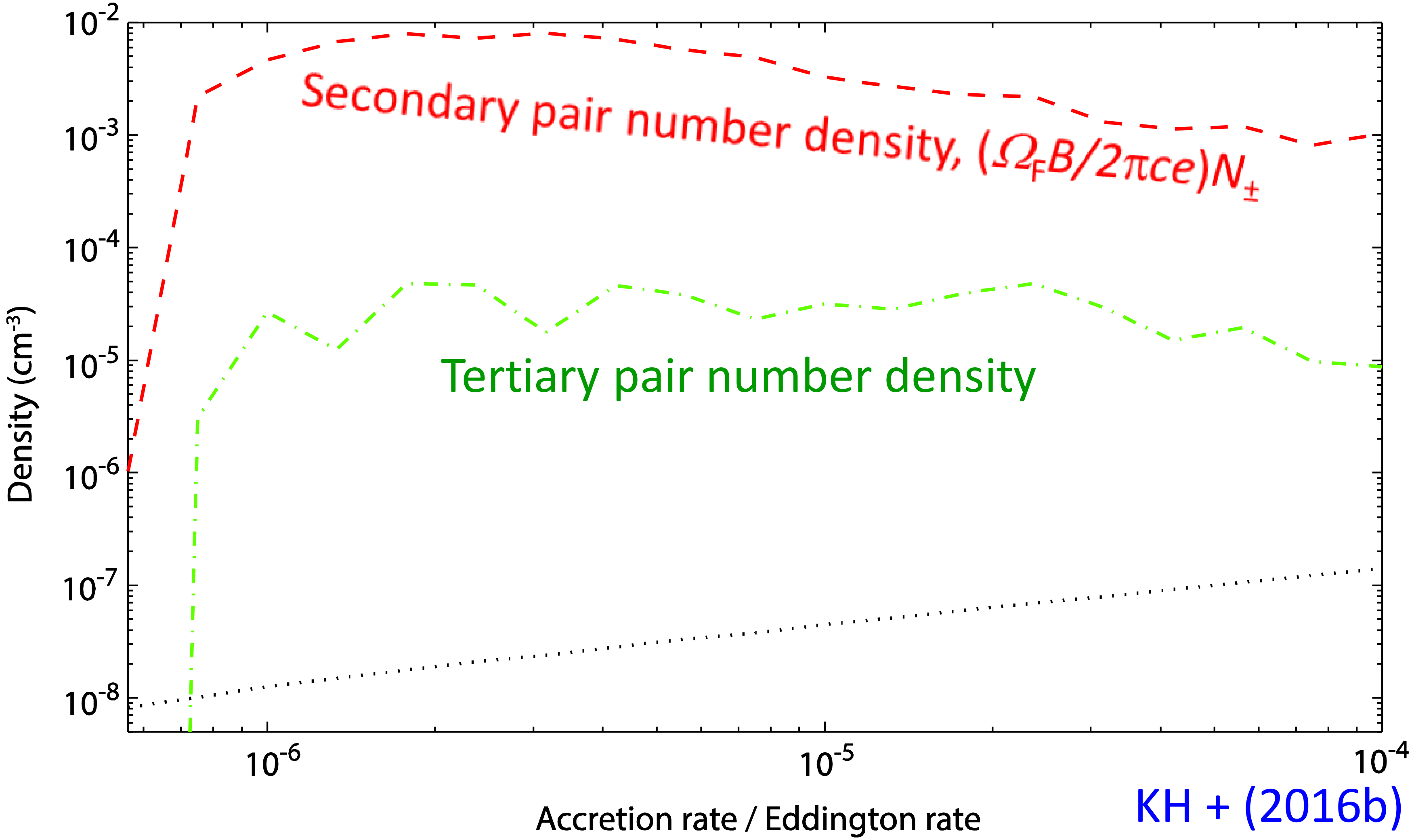

KH + (2016b)

§ 6 Results: Intermediate-mass BHs

For IMBH, $M=10^5 M_\odot$, $B=B_{eq}$; SED @ five m's.

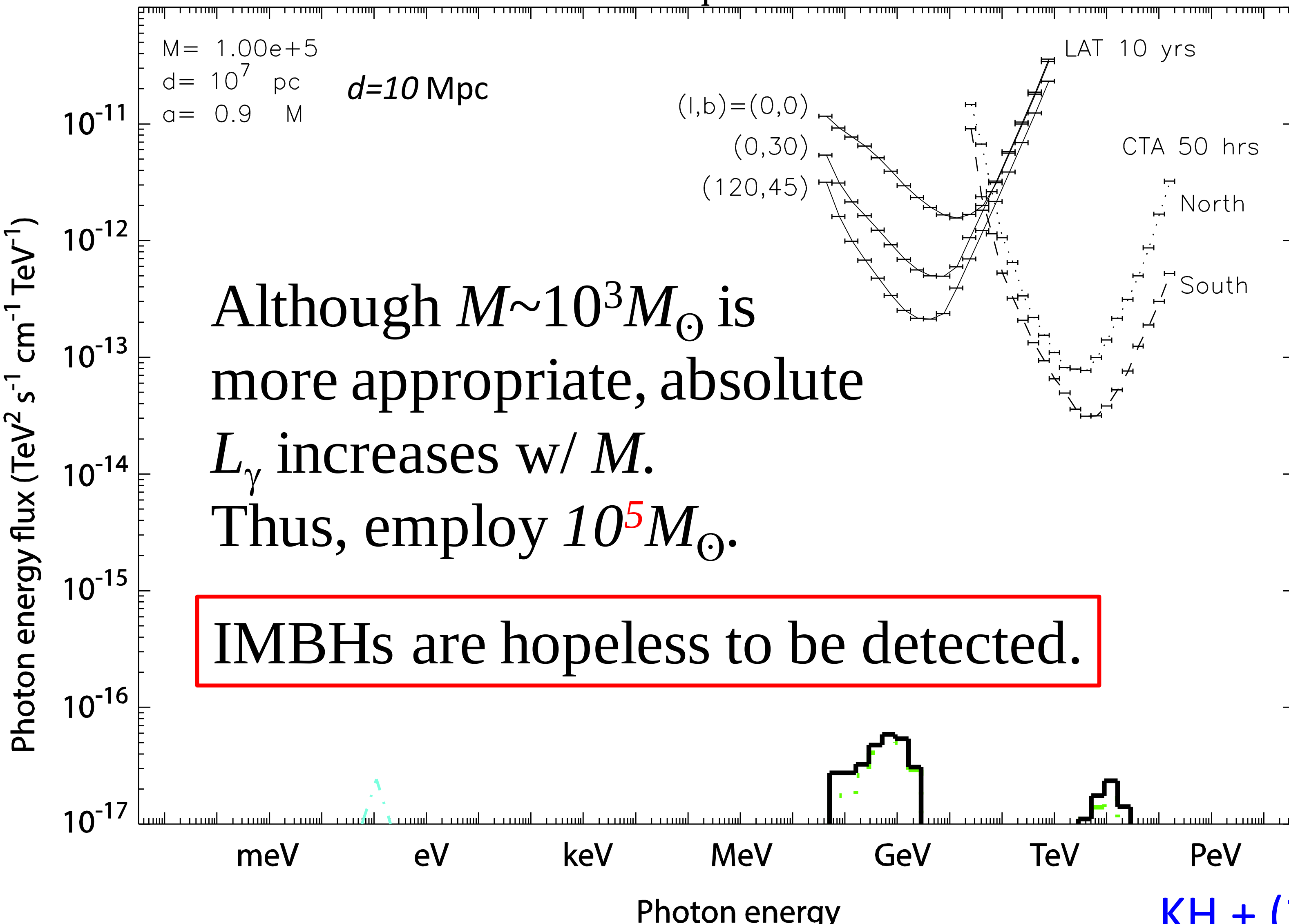

Although $M \sim 10^3 M_\odot$ is more appropriate, absolute L_γ increases w/ M.
Thus, employ $10^5 M_\odot$.

IMBHs are hopeless to be detected.

KH + (2016b)

§ 6 Results: IMBHs

$M=10^5 M_\odot$, $B=B_{eq}$; Curvature vs. IC luminosity ($\theta=0^o$)

Curvature » IC @ $\dot{m}<2\times10^{-5}$.

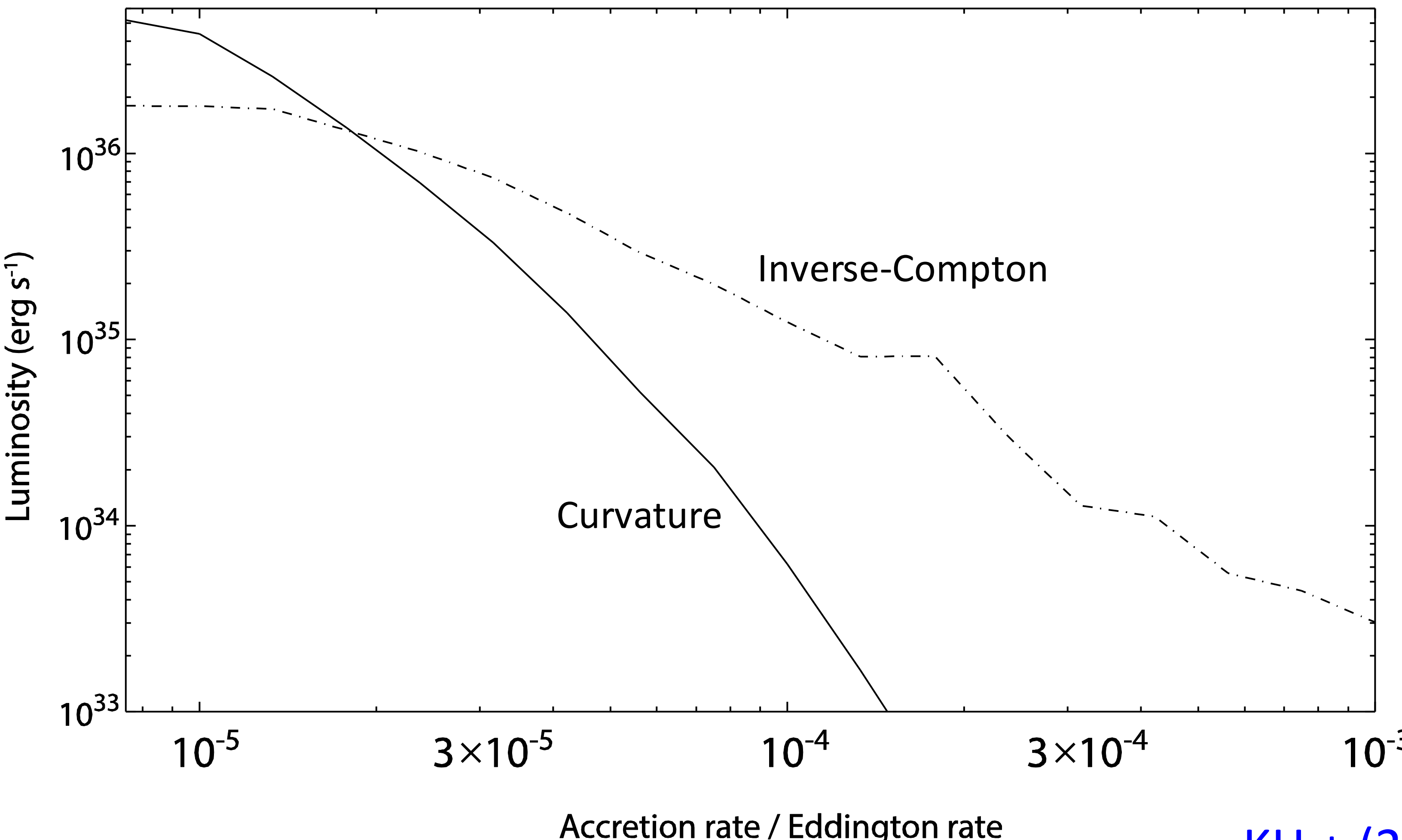

KH + (2016b)

§ 6 The case of IMBHs

M=$10^5 M_\odot$, B=B_{eq}; Cascaded pair density » GJ @ $\forall \dot{m}$.

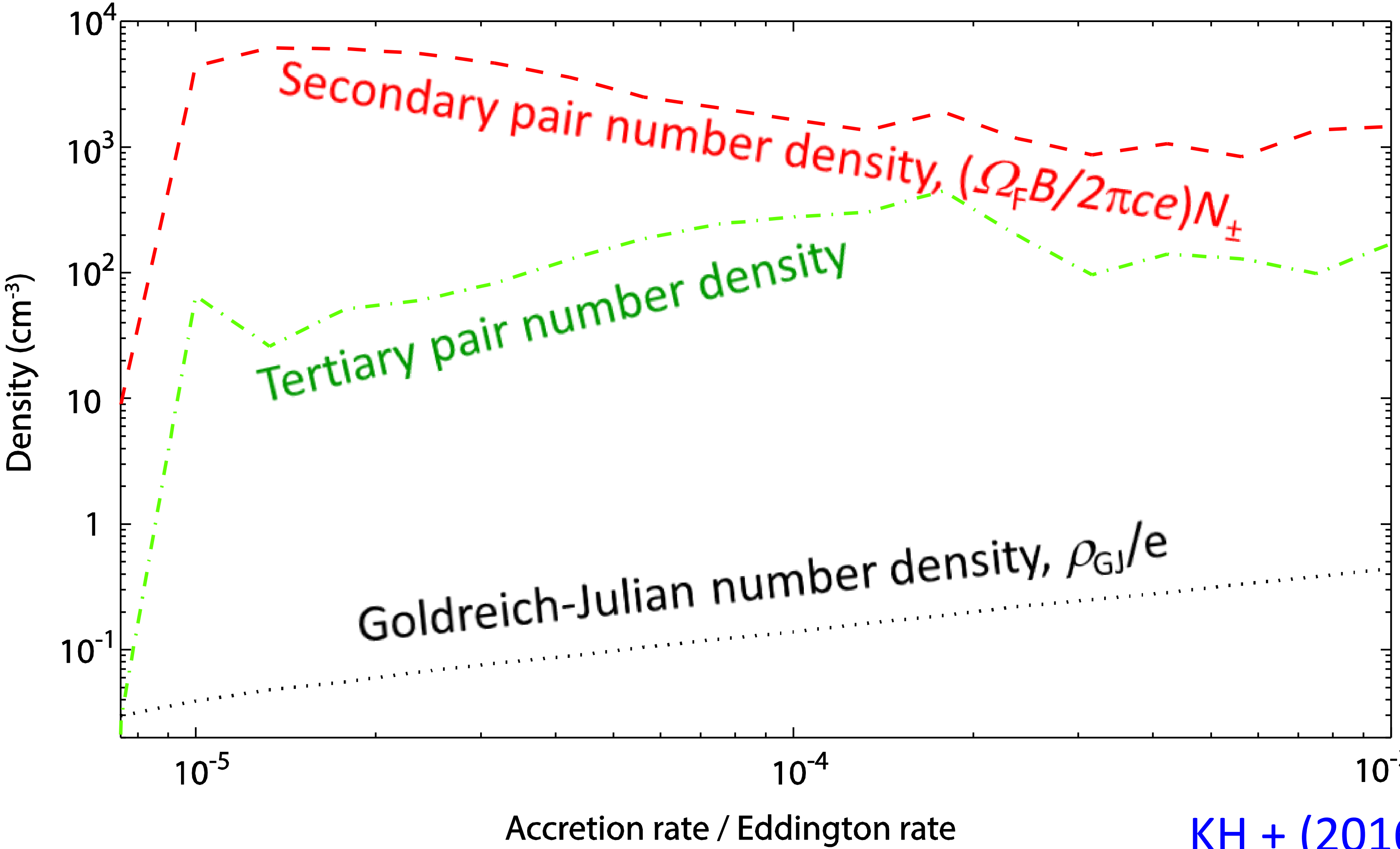

KH + (2016b)

§ 7 Detectability: black hole transients

J0620-0020: detectable in HE & VHE during quiescence.

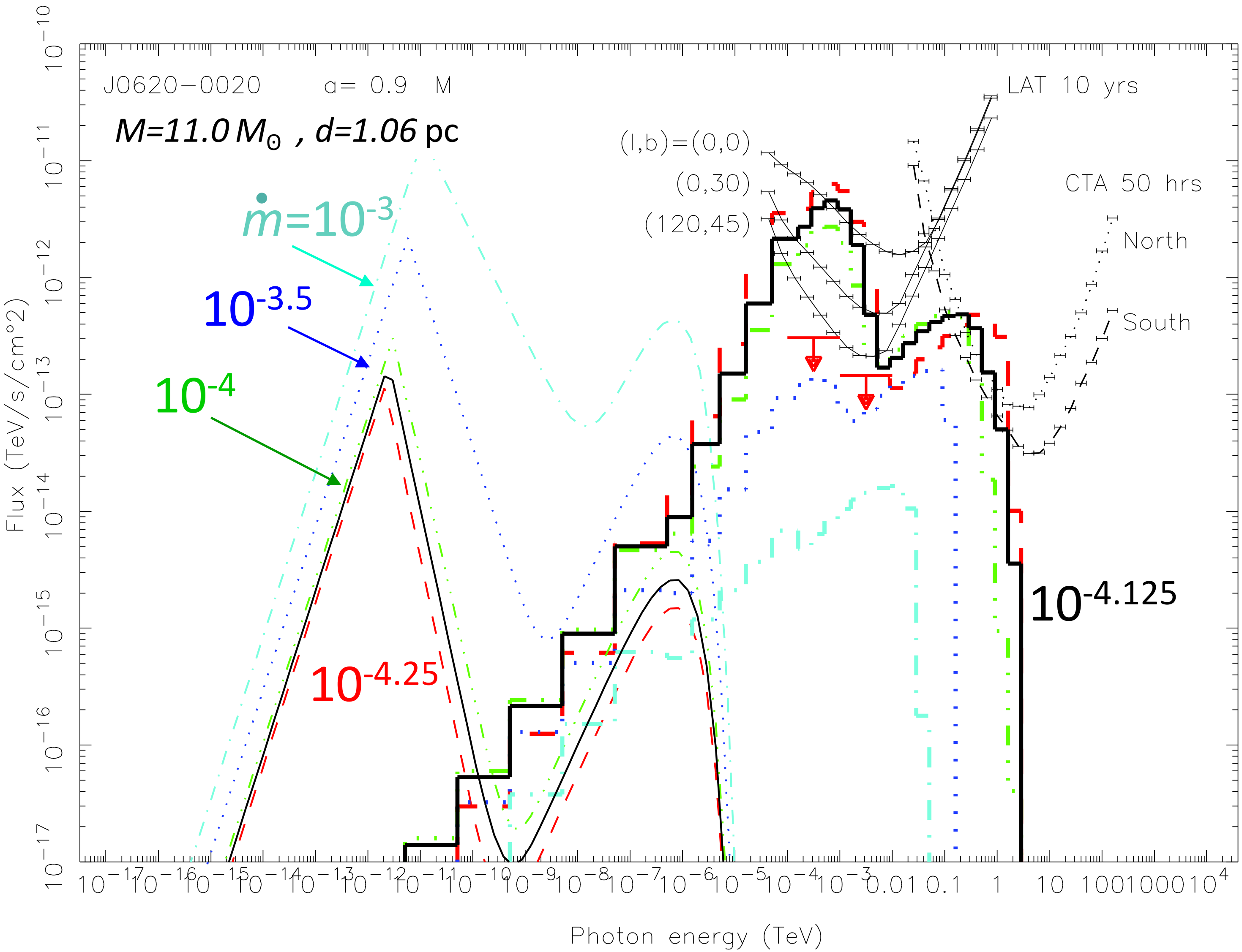

However, reanalysis of LAT 7 yrs data gives stronger constraint, setting upper limit of flaring duty cycle.

Lin + ('16), in prep.

§ 7 Detectability: black hole transients

GRO J1655-40: maybe detectable in HE during quiescence.

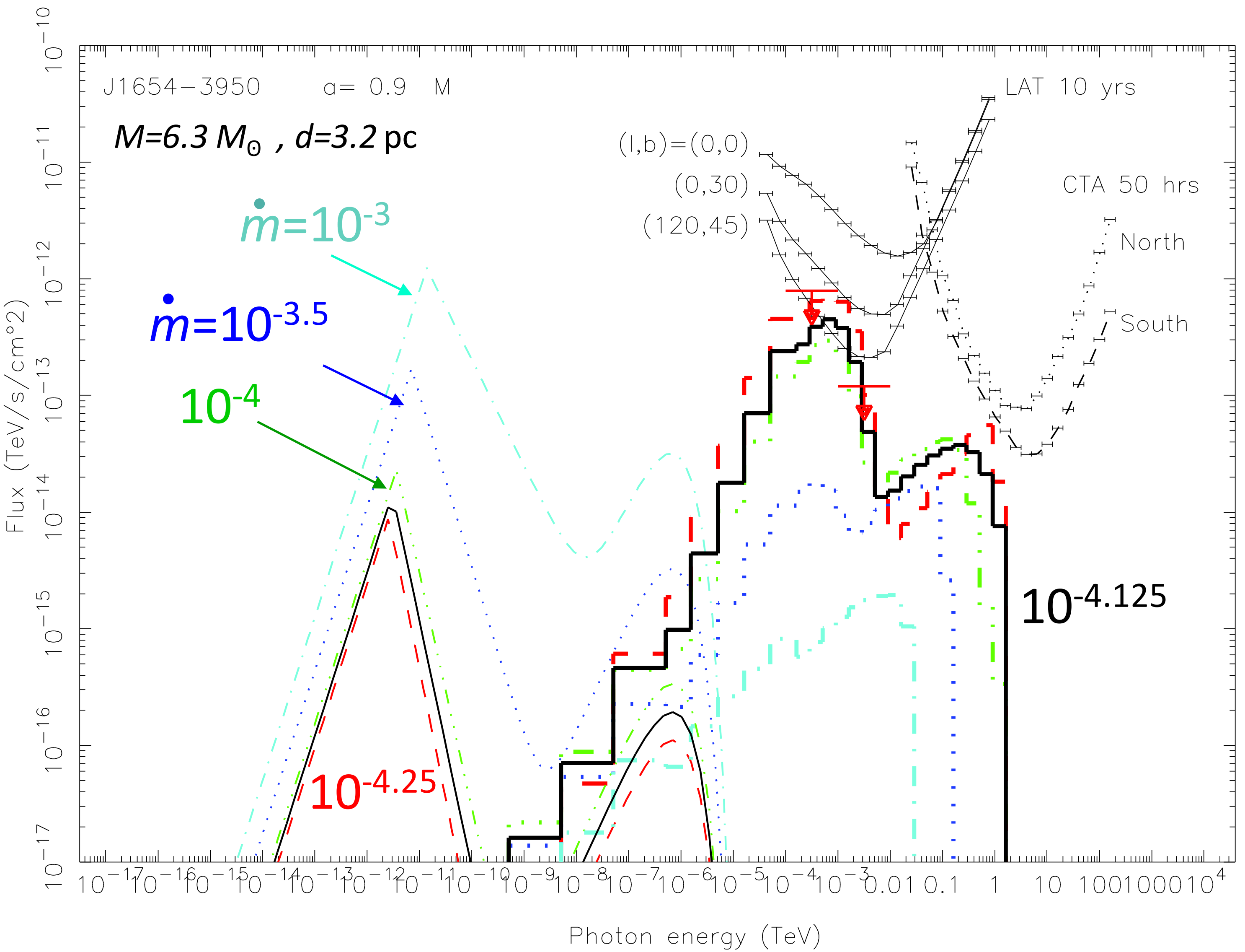

Lin + ('16), in prep.

§ 7 Detectability: black hole transients

XTE J1752-223: difficult to be detected in HE.

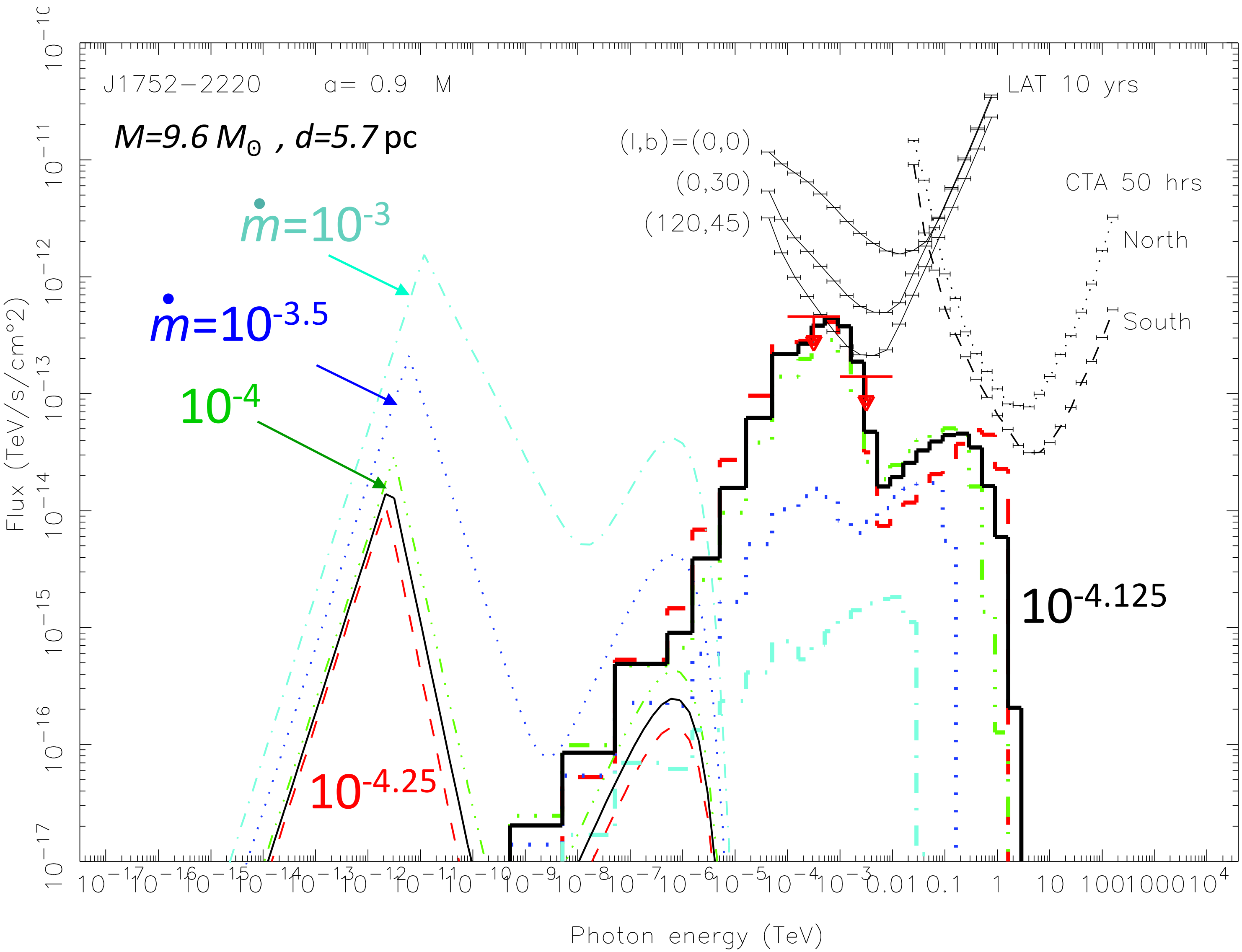

Lin + ('16), in prep.

§ 7 Detectability: black hole transients

V404 Cyg: marginally detectable in HE during quiescence.

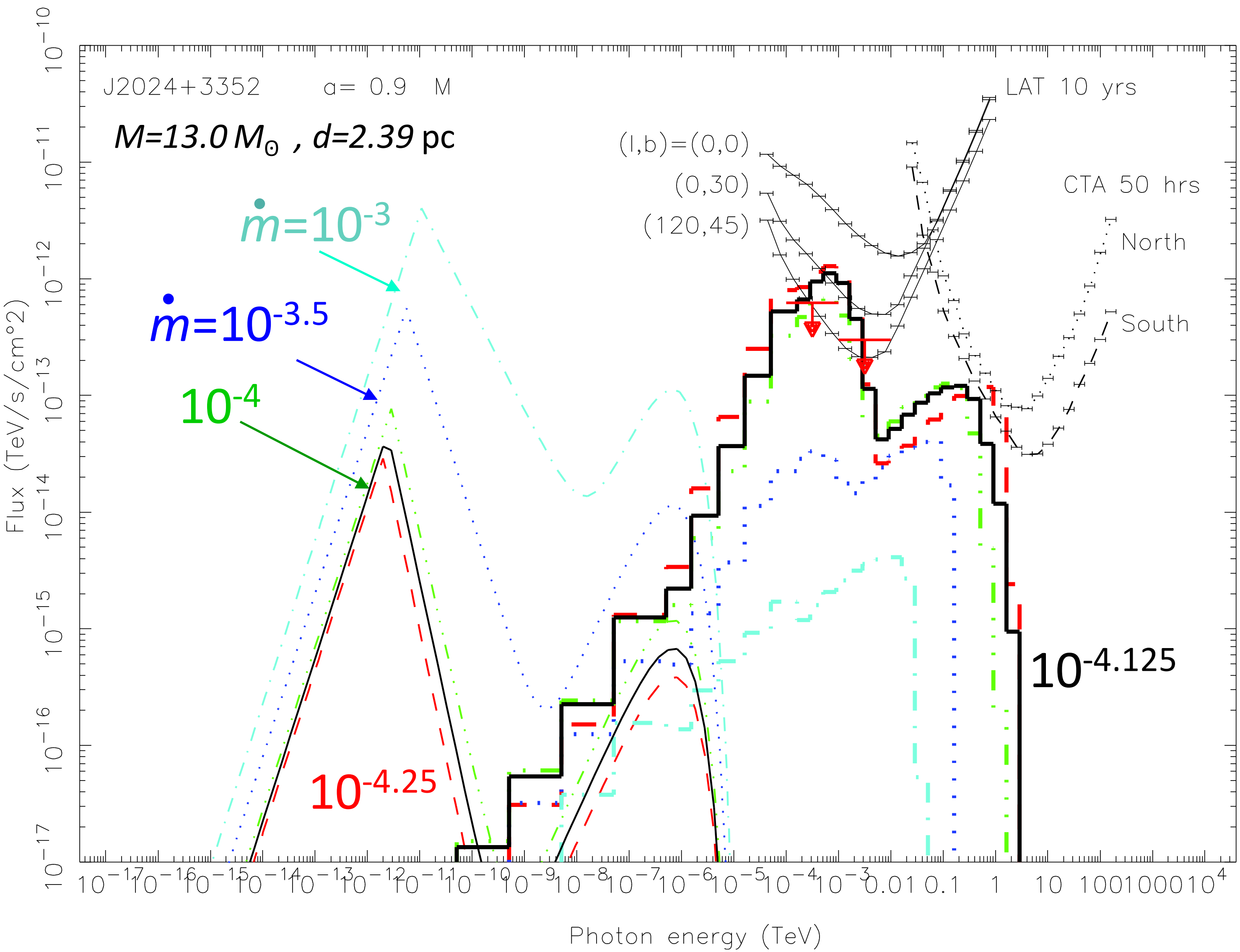

Lin + ('16), in prep.

§ 7 Detectability: black hole transients

J1118+4802: detectable in HE during quiescence.

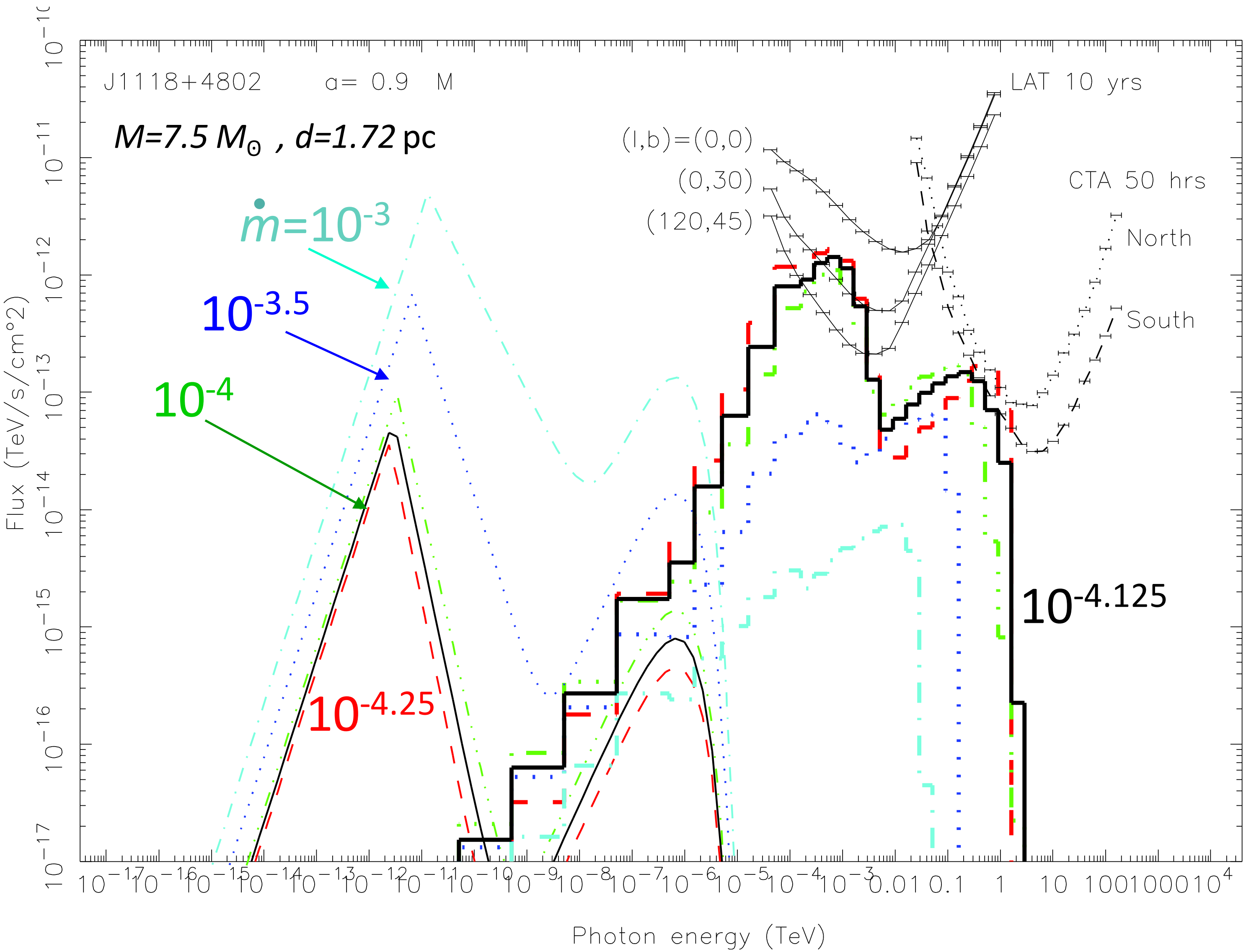

§ 7 Detectability: black hole transients

J1650-4957: difficult to be detected (on galactic plane).

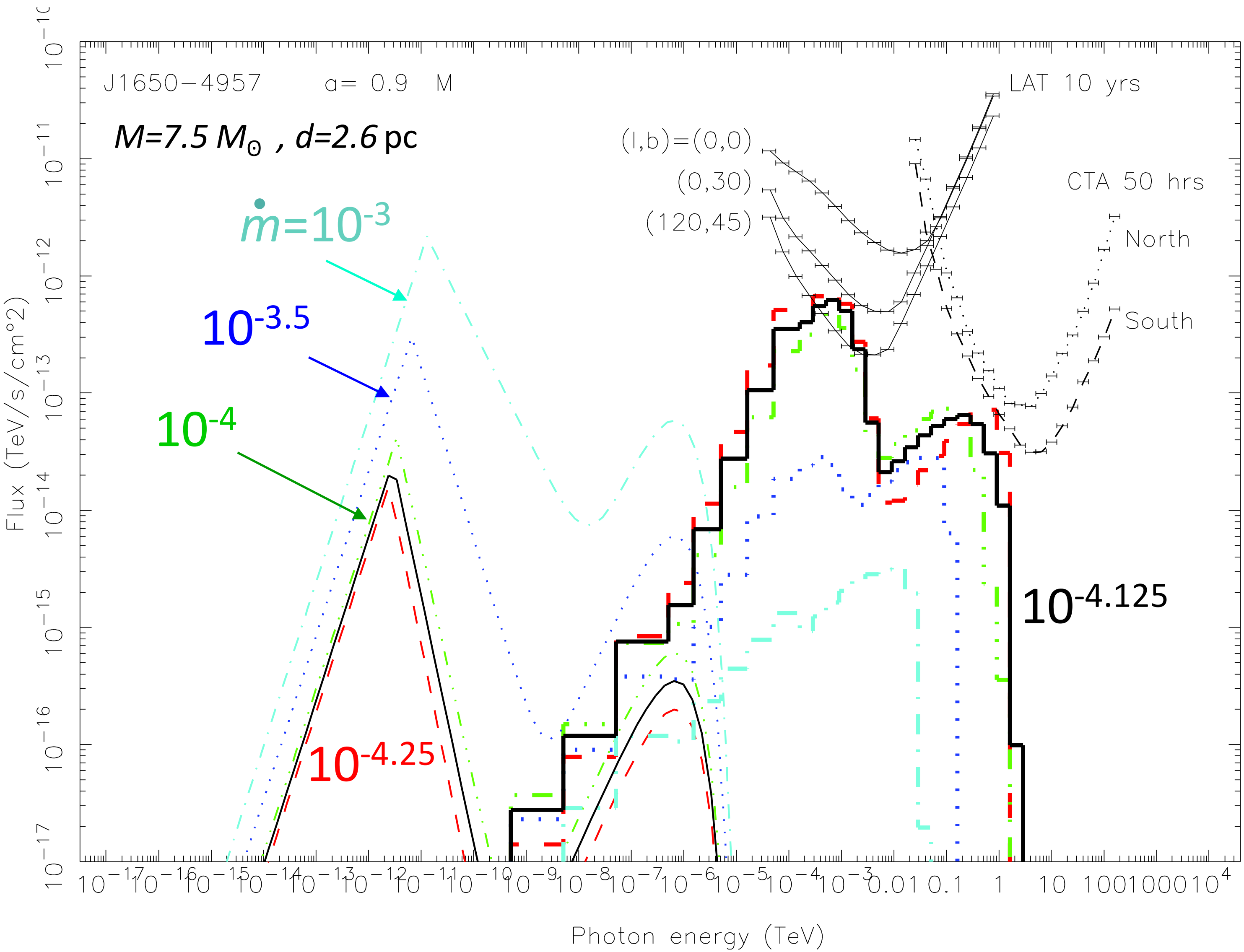

§ 7 Detectability: black hole transients

GX339-4: Hopeless to be detected.

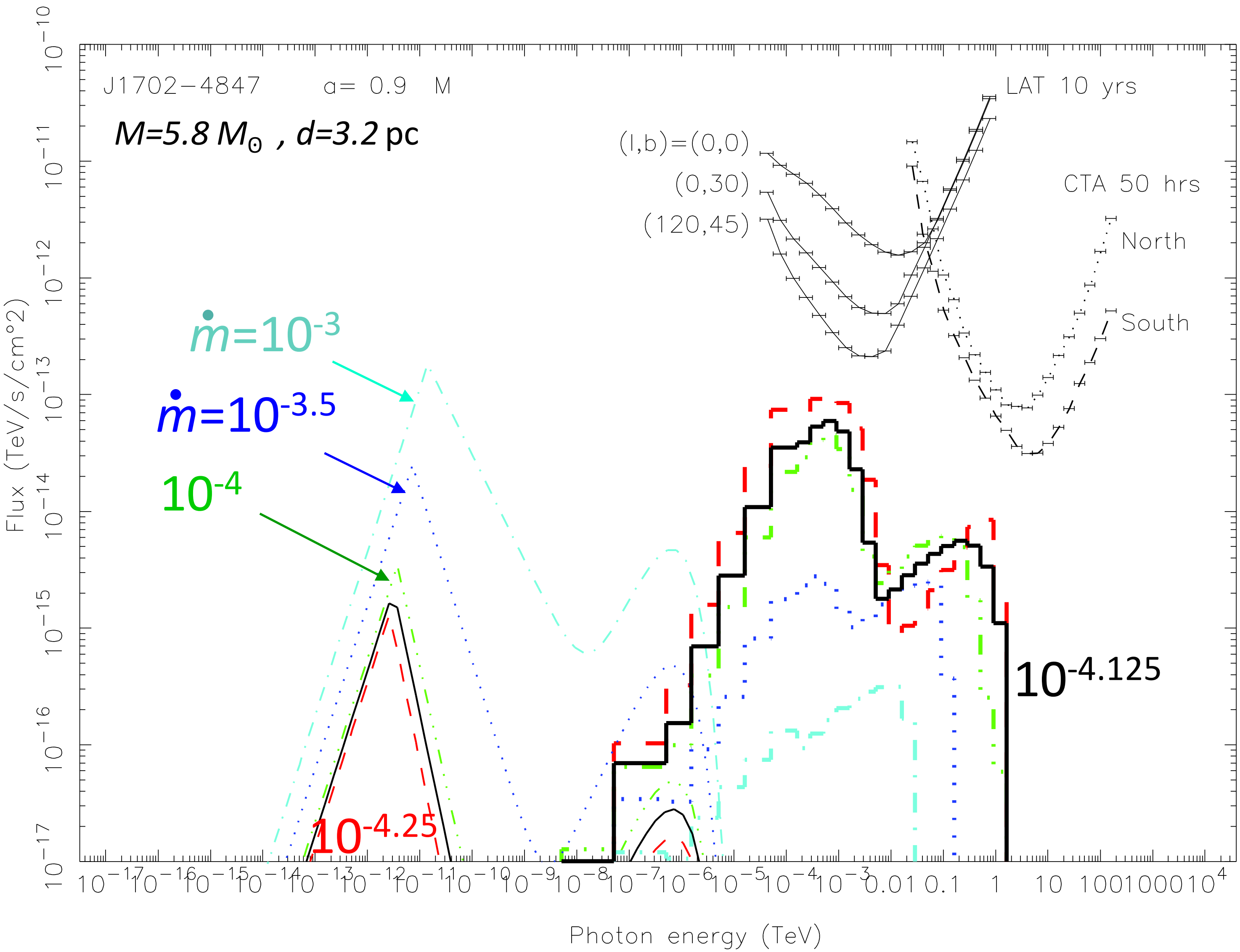

Summary on BH gap model

- If $\dot{m} < \dot{m}_{\rm up} = 3\times10^{-3} M_1^{-0.14}$, gap appears near the horizon, dissipating a part of BH's rotational energy.
- In the gap, $e^{\pm}$'s are accelerated to $\gamma \sim 10^7$ for stellar-mass BHs.
- For stellar-mass BHs, curvature photons appear at ~GeV and are detectable w/ Fermi/LAT during quiescent.
- For stellar-mass BHs, primary & secondary IC photons appear at 3-30 TeV and are detectable w/ CTA.
- For SMBH, primary IC photons (3-30 TeV) are marginally detectable w/ CTA.
- We can discriminate gap vs. jet emissions by anti-correlation vs. correlations at IR/opt & HE/VHE. Thus, simultaneous observations of BH transient(s) at IR/opt & VHE are necessary.